RNA binding regulates TRIM25-mediated RIG-I ubiquitylation

Kevin Haubrich[1,2], Sandra Augsten[1], Bernd Simon[1], Pawel Masiewicz[1], Kathryn Perez[3], Mathilde Lethier[4], Katrin Rittinger[5], Frank Gabel[6], Stephen Cusack[4], Janosch Hennig[1,*]

[1] Structural and Computational Biology Unit, EMBL Heidelberg, Meyerhofstraße 1, 69117, Heidelberg, Germany
[2] Collaboration for joint PhD degree between EMBL and Heidelberg University, Faculty of Biosciences
[3] Protein Expression and Purification Core Facility, EMBL Heidelberg, Meyerhofstraße 1, 69117, Heidelberg, Germany
[4] European Molecular Biology Laboratory, 71 Avenue des Martyrs, 38042, Grenoble, Cedex 9, France
[5] Molecular Structure of Cell Signalling Laboratory, The Francis Crick Institute, 1 Midland Road, London, NW1 1AT, UK
[6] University Grenoble Alpes, CEA, CNRS, IBS, 71 avenue des Martyrs, 38044, Grenoble, France

* To whom correspondence should be addressed. Tel: +49 6221 387-8552; Email: janosch.hennig@embl.de

ABSTRACT

TRIM25 is a ubiquitin E3 ligase active in innate immunity and cell fate decisions. Mounting evidence suggests that TRIM25's E3 ligase activity is regulated by RNAs. However, while mutations affecting RNA-binding have been described, the precise RNA binding site has not been identified nor which domains are involved. Here, we present biophysical evidence for the presence of RNA binding sites on both TRIM25 PRY/SPRY and coiled-coil domains, and map the binding site on the PRY/SPRY with residue resolution. Cooperative RNA-binding of both domains enhances their otherwise transient interaction in solution and increases the E3 ligase activity of TRIM25. Mutational analysis shows that RNA binding affects ubiquitination of RIG-I in mammalian cells. In addition, we present a simple model system for RNA-induced liquid-liquid phase separation of TRIM25 *in vitro*, resembling previously observed cellular RNA granules, that facilitates the recruitment of RIG-I.

INTRODUCTION

TRIM25-mediated RIG-I signaling is one of the key steps in the host response against a broad spectrum of RNA viruses, many of which pose a significant hazard for public health and human well-being, such as Influenza, Dengue, Ebola and the novel coronaviruses (1). Many of these viruses have developed host-pathogen interactions to evade host immunity by interfering with TRIM25-mediated RIG-I ubiquitination (2-7). The recent outbreaks of emerging human pathogens such as Ebola in Western Africa in 2013-2016 or the ongoing SARS-CoV-2 pandemic, the steady rise in Dengue virus infections over the last 50 years as a consequence of human-made climate change, as well as the seasonal death toll caused by Influenza virus, which could be significantly increased in the event of a pandemic, highlight the importance of understanding these host-pathogen interactions as a potential target for fighting these diseases.

In this study we focus on the role of RNA binding of the E3 ligase TRIM25 in its physiological functions and its exploitation by viruses in host immunity evasion (8-11). TRIM25 is part of the tripartite motif (TRIM) family of ubiquitin ligases characterized by an N-terminal RING domain, followed by one or two B-box domains, a coiled-coil (CC) dimerization domain and a C-terminal region, which, depending on the subfamily, can feature various domains (Figure 1A). TRIM25 is a member of the PRY/SPRY domain subfamily and the first member of this subgroup where RNA binding has been

observed (6,12-14). TRIM25 has reported functions in innate immunity, morphogenesis and cell proliferation (15-19), but mechanistic understanding of its mode of action is scarce.

The best characterized function of TRIM25 is its role in RIG-I signalling during the antiviral response. Here, it ubiquitinates the RIG-I caspase activation and recruitment domains (CARDs), which are exposed upon recognition of 5′ triphosphate blunt-end double-stranded RNA (15,20-22). The importance of this pathway in innate immunity is highlighted by the variety of mechanisms that viruses have evolved to inhibit TRIM25 activity and evade the host defense (2-7). TRIM25 has been shown to also ubiquitinate other targets, often RNA-binding proteins. In embryonic stem cells, TRIM25 is required for the binding of Lin28a to the precursor of let-7 (pre-let-7), which in turn recruits Tut4 to the RNA (23). Tut4, after activation through ubiquitination by TRIM25, poly-uridylates pre-let-7 and thereby marks it for degradation. Also, TRIM25 ubiquitinates the zinc-finger antiviral protein (ZAP), a protein interacting with viral mRNA and facilitating exosome-mediated degradation (24). Various RNAs seem to act as co-factors for TRIM25's E3 ubiquitin ligase activity, facilitating auto-ubiquitination and ubiquitination of RIG-I and ZAP (25-27). While most studies point towards an activating role of RNA on TRIM25 *in vitro*, there is some evidence that the Dengue virus uses its subgenomic RNA to inhibit TRIM25 and its role in interferon expression (3).

Despite clear evidence for the importance of RNA-binding for TRIM25 activity, the molecular mechanism of this activation remains unexplained and structural data on the TRIM25-RNA interaction is lacking. The identity of the RNA-binding domain also remains controversial, with the CC domain originally being identified (12), while more recent data point towards the PRY/SPRY domain (25). In addition, a lysine-rich part of the linker connecting CC and PRY/SPRY domain was proposed to be involved in this interaction (26). Here, we resolve this controversy by showing that the CC and PRY/SPRY domains act together cooperatively to bind RNA. We have previously shown that the PRY/SPRY and CC interact weakly in solution (28) and that this interaction is necessary for RIG-I ubiquitination. Binding to RNA enhances the CC-PRY/SPRY interaction, mechanistically explaining the observed activation of TRIM25 E3-ubiquitin ligase activity. Functional assays in mammalian cells confirm the importance of RNA binding interfaces on both domains, as RNA binding mutants lessen RIG-I ubiquitination. RNA-binding also induces the formation of macromolecular condensates (liquid-liquid phase separation) *in vitro* and recruits RIG-I CARDs into these condensates. TRIM25 also forms condensates in cells. This suggests a completely new molecular mechanism of TRIM25/RIG-I interaction in which a common RNA acting as a scaffold rather than direct protein/protein-interactions is critical to bring the two proteins together.

MATERIAL AND METHODS

Protein expression and purification

TRIM25 CC (aa 189-379), PRY/SPRY (439-630) and CC-PRY/SPRY (189-630) were cloned using restriction free cloning into pETM22 featuring a 3C-protease cleavable hexa-histidine and thioredoxin tag (His-Trx). An alternative N-terminally extended PRY/SPRY construct (407-630) was cloned into

pETM20 with a TEV-protease cleavable His-Trx tag. TRIM25 189-379 was expressed in BL21(DE3). TRIM25 439-630, 407-630 and 189-630 were co-expressed with chaperones KJE, ClpB and GroELS in *E. coli* BL21(DE3) (29). All proteins were induced at OD600=0.6 by 200 µM isopropyl-ß-D-1-thiogalactopyranoside (IPTG) and incubated at 18˚ C for 20h.

All proteins were purified by immobilized Nickel affinity chromatography (GE Histrap FF) in 50 mM Tris, pH 7.5, 300 mM NaCl and 0.2 mM TCEP and eluted with a gradient of imidazole (10-300 mM). In the case of coexpression with chaperones the column was washed with 50 mM Tris, pH 7.5, 350 mM KCl, 5 mM MgSO4 and 1 mM ATP prior to elution. The tag was removed by TEV-protease digestion overnight and an additional passage over the HisTrap column (189-379 and 407-630) or GE HiTrap SP HP cation exchange column (PRY/SPRY, residues 439-630 and CC-PRY/SPRY, residues 189-630). As a final step aggregates were removed by gel filtration on a GE Superdex S75 (CC, PRY/SPRY, extended PRY/SPRY) or S200 (CC-PRY/SPRY) in 20 mM MES, pH 6.5, 75 mM NaCl and 0.5 mM TCEP. For stable isotope labelling, proteins were expressed in M9 medium using $^{15}NH_4Cl$ (0.5 g/l) or $^{15}NH_4Cl$ /^{13}C-Glucose (2 g/l) as sole nitrogen and carbon source.

Human RIG-I CARDs (residues 1-203 and 1-208) were cloned into pETM11 using the NcoI and KpnI sites, expressed in BL21(DE3) Rosetta 2 and induced with 250 µM IPTG overnight at 16 ˚C. The protein was purified using a Qiagen Nickel NTA superflow column in 25 mM Tris pH 7.5, 150 mM NaCl, 10% glycerol, 0.5 mM TCEP. The column was washed with 20 mM imidazole and 1 M salt and the protein eluted with 300 mM imidazole in the same buffer. The tag was removed by TEV-protease cleavage and an additional passage over the Ni-NTA column. Residual aggregates were removed in a final size exclusion chromatography step on a Superdex 75 column (GE healthcare) in a buffer containing 25 mM HEPES pH 7.5, 150 mM NaCl, 0.3 mM TCEP. dTomato-tagged RIG-I CARDs construct (aa 2-200) was cloned into pETM11 and expressed in *E. coli* BL21(DE3) with 0.4 mM IPTG at 18˚ C for 20h. The protein was purified by Nickel affinity chromatography and subsequent size exclusion chromatography using a Superdex S200 in 20 mM Hepes, pH 7.5, 100 mM NaCl, 0.2 mM TCEP.

RNA production

pre-let-7a-1@2 (5'-GUA UAG UUU AAA AGG AGA UAA CUA UAC -3') and DENV-SL (5'- GCA GGU CGG AUU AAG CCA UAG UAC GGG AAA AAC UAU GCU ACC UG-3') were *in vitro* transcribed from DNA oligos using T7 RNA polymerase. Reaction mixtures containing 2 µM forward and reverse primer, 40 mM Tris, pH 8.0, 0.2 mM MgCl2, 10 mM spermidine, 15 mM DTT, 0.01 % Triton X-100, 4 U/ml TIPP, 0.1 mg/ml T7 polymerase were incubated for 5 hours at 37˚ C and extracted by chloroform/phenol treatment. The aqueous phase was further purified by preparative gel electrophoresis via denaturing PAGE or HPLC using a Thermo DNA Pac PA100 22x250mm anion exchange column at 95˚ C. The purified RNA was dialyzed against 20 mM MES, pH 6.5, 75 mM NaCl and 0.5 mM TCEP and refolded before use by heating up at 95˚ C for 5 minutes and snap-cooling on ice. Solid-phase synthesized Lnczc3h7a (5'-UUUUAUCUGAGUUGGAGGUGAAG-3') and the shorter

pre-let-7 loop (5'-UAA AAG GAG AU-3') and stem (5'-GUA UAG UUC AAC UAU AC-3') constructs were purchased from IBA.

Nuclear magnetic resonance spectroscopy

NMR spectra were acquired on Bruker Avance III spectrometers operating at magnetic field strengths corresponding to proton Larmor frequencies of 600, 700, and 800 MHz, equipped with a cryogenic triple resonance probe (600 and 800 MHz) and a room temperature triple resonance probe (700 MHz). All experiments were performed in 20 mM sodium phosphate, pH 6.5, 150 mM NaCl, 2 mM TCEP, 5% D_2O and 0.02% sodium azide at 293 K. For titrations 100 µM ^{15}N-labelled TRIM25 407-630 or 439-630 were titrated with stock solutions of 10-20 mM natural abundance RNA or 250-300 µM RIG-I CARDs (1-203 or 1-209) to a molar excess of 2.5-3 (details indicated in the figures). At each titration point a ^{1}H-^{15}N-HSQC spectrum was acquired. Spectra were processed using NMRPipe (30), visualized and peak shifts tracked using SPARKY (31). Peak shifts for PRY/SPRY 439-630 were assigned based on a previously published assignment (28). For PRY/SPRY 407-630, peak assignments were transferred from PRY/SPRY 439-630 and confirmed and extended, using HNCA and HNCACB backbone assignment experiments. Secondary structure and order parameters were estimated from chemical shifts using TALOS and Sparta+ (32,33). R_1 and R_2 relaxation rates and $\{^{1}H\}/^{15}N$ heteronuclear NOEs were recorded using standard pulse sequences and analysed using PINT (34-36). Relaxation delays of 20, 50, 100, 150, 250, 300, 400, 500, 650, 800, 1000, 1300, 1600, 2400 ms for the R_1 experiment and 16, 32, 48, 64, 80, 96, 128 ms for the R_2 experiment were used.

Isothermal titration calorimetry

Isothermal titration calorimetry (ITC) data was collected on a Malvern MicroCal PEAQ-ITC at 20˚ C in 20 mM MES, pH 6.5, 75 mM NaCl and 0.5 mM TCEP. Depending on the protein construct, RNA was titrated from the syringe at concentrations ranging from 20-860 µM into the cell containing protein with concentrations between 2-150 µM while stirring at 750 rpm (see Figure 2 and Supplementary Figure S3). For experiments with DENV-SL the RNA was kept in the cell at 15 µM and the protein titrated from the syringe at 110 µM. Experiments were typically done in triplicates and analysed using the MicroCal PEAQ-ITC analysis software. Data was fitted by assuming the simplest binding mode necessary to fully explain the data (one or two binding sites).

Small-angle X-ray scattering

SAXS data were collected at the beamline P12, operated by EMBL Hamburg at the PETRA III storage ring (DESY, Hamburg, Germany) (37). Measurements were done at 20 °C in 20 mM MES, pH 6.5, 75 mM NaCl and 0.5 mM TCEP in flow cell mode at 1.24 Å. For each sample and buffer 20-100 frames with 0.05-0.195 s exposure time were acquired and frames showing radiation damage manually removed. Data analysis was done using the ATSAS package version 2.8.3 (38). PRIMUS was used for frame averaging and buffer subtraction (39). The radius of gyration, R_g, was estimated using the Guinier approximation in PRIMUS. Pair-wise distribution functions were calculated using GNOM (40). Collection statistics for SAXS measurements are summarized in Supplementary Table S1.

Filter binding assays

Filter binding assays were carried out in 200 µl of binding buffer (20 mM MES, pH 6.5, 75 mM NaCl, 0.5 mM TCEP). Structured RNA probes were refolded prior to experiments by heating at 85°C for 3 min and slow cooling to room temperature. A concentration series of TRIM25 CC-PRY/SPRY was incubated with 5' ^{32}P-labelled RNA for 10 min on ice and the sample were filtered through Whatman 0.45µm nitrocellulose filters. The protein/RNA complex was retained on the filters and detected by scintillation counting. Binding curves were fitted using SciDavis as:

$$A(c_{protein}) = \frac{A_{max} \times c_{protein}}{K_D + c_{protein}}$$

Where A_{max} and $A(c_{protein})$ are measured activities. This approach only gives valid results, if the K_D is much smaller than the concentration of radio-labelled RNA. In cases, were this assumption was false the K_D was corrected as follows:

$$K_D = K_D^{fit} - \frac{c_{RNA}}{2}$$

In cell ubiquitination assays

In cell ubiquitination of RIG-I CARDs by TRIM25 and its mutants was assessed as previously described (28). In short, HEK293T cells were cultured in DMEM with 10% FBS and antibiotics and seeded in 6 well plates ($5x10^5$ cells per well) 24 hours prior transfection. Cells were transfected using Fugene transfection reagent and the respective expression constructs (RIG-I 2-200 with N-terminal FLAG-tag, TRIM25 full-length WT and mutants) in a pcDNA3 expression vector.

24h after transfection cells were lysed in IP-lysis buffer (50mM Tris, 150mM NaCl, 5mM $MgCl_2$, 0.5% IGEPAL, protease inhibitors). For proteasome inhibition, cells were treated with increasing concentrations of carfilzomib (100 – 1000nM) 24 hours after transfection and lysed as before after additional 24 hours. An aliquot of the lysates was used for western blot to test and quantify the overexpression of TRIM25 and FLAG-RIG-I CARDs.

Immunoprecipitation (IP) using aFLAG magnetic beads were performed using similar amounts of lysate. IP was done to enrich overexpressed FLAG-RIG-I CARDs to investigate their ubiquitination state. IP eluates were used for western blot against FLAG-tag and ubiquitin. Experiments were done at least in triplicates. Ratios of ubiquitinated to unmodified CARDs were quantified, normalized to their counterpart in the lane with no exogenous TRIM25 expression, averaged and the standard deviation calculated.

Live cell imaging and image analysis

HeLa cells were cultured in DMEM with 10% FBS and antibiotics and seeded in glass bottom plates ($3x10^5$ cells per well) 24 hours prior transfection. Cells were transfected using Fugene transfection reagent and the respective expression constructs for mEGFP-TRIM25 and dTomato-RIG-I CARDs (aa 2-200) in pcDNA3. Oxidative stress was induced by treatment with 0.5 mM sodium (meta)arsenite for 2 hours. Cells were imaged at 37 ˚C on an Olympus FV3000 inverted confocal microscope equipped with an Olympus UPL SAPO 40x2 NA 0.95 objective.

In vitro phase separation assays

TRIM25 CC-PRY/SPRY (WT or K283A/K285A/H505E/K508E/K602E pentamutant) and DENV-SL or pre-let-7 were mixed in equimolar ratios at concentrations between 1 and 10 µM in 20 mM sodium phosphate, pH 6.5, 100 mM NaCl and 0.5 mM TCEP at room temperature and immediately imaged using differential interference contrast (DIC) on an Olympus FV3000 inverted confocal microscope and Olympus UPL SAPO 40x2 NA 0.95 objective. To assess localisation of RIG-I with TRIM25/DENV-SL, bacterially expressed dTomato-RIG CARDs or dTomato alone were added at 3 µM to macromolecular condensates pre-formed at 5 µM and distribution of dTomato was observed by confocal fluorescence microscopy. Fluorescence intensity as a measure of protein concentration in the droplets and surrounding media was quantified using Fiji (41). For each condition fluorescence intensity was measured for at least twenty droplets and an equivalent number of points in the surrounding media distributed over at least three frames, normalized by the average intensity of the frame, averaged and plotted using SciDavis.

RESULTS

Two distinct sites of the TRIM25 PRY/SPRY domain bind to single and double stranded RNA

Since RNA-binding of TRIM25 is structurally uncharacterized, we performed NMR titrations with the TRIM25 PRY/SPRY domain and the reported RNA target pre-let-7a-1 (Figure 1B). A minimal pre-let-7a-1@2 construct (pre-let-7 in the following) has been described to promote TRIM25-mediated regulation of let-7 by Lin28a and TuT4 (23). Upon addition of RNA we observed strong chemical shift perturbations (CSPs) clustered around two regions of the PRY/SPRY domain (Figure 1B-D). The first of the two binding sites (binding-site-1 in the following) is located at the C-terminus of the PRY motif with the strongest affected residues in the flexible loop connecting ß-strands 3 and 4 (Supplementary Figure S1). This site is located in close proximity to the interaction site between the PRY/SPRY and CC reported in Koliopoulos *et al.* (28). Our data thereby confirm the RNA-binding region (aa 470-508) reported by Choudhury *et al.* (25), but increase the accuracy to residue resolution. The second binding site is located in a region formed by ß-strands 10 and 11 and is located close to the N-terminal helix α1 (Supplementary Figure S1). Although this region was not shown earlier to be involved in RNA binding, a central role in the recruitment of RIG-I has been reported (42). At this stage, we could not assess, whether the CSPs are due to direct interaction with RNA or due to an allosteric effect.

To further assess RNA specificity of these binding sites we designed shorter RNA constructs consisting of only the loop or stem of pre-let-7 (Supplementary Figure S2). Upon titration with the single stranded part of pre-let-7 (pre-let-7 loop), we observed CSPs only for residues located at binding-site-1, whereas binding-site-2 was unaffected (Figure 1E). To ensure that the short stem is double-stranded, we fused the strands together by a three bases long linker (pre-let-7 stem). Titration with the resulting RNA construct strongly affected both binding sites, 1 and 2 (Figure 1F). Together this suggests that the second binding site is specific for double-stranded RNA, while the first binding site seemingly binds to single- and double-stranded RNA. The presence of two binding sites with distinct binding preferences in close proximity suggests a possible binding selectivity for structural elements rather than sequence specificity. Indeed, comparing other reported RNA targets of TRIM25, we found that all feature stem loops of similar size and sequence as pre-let-7. We used ITC to measure the affinity of several of these stem loops to TRIM25 CC-PRY/SPRY (Table 1). We observed very tight binding of this construct to pre-let-7 ($K_{D\ =}$ 72 ± 33nM, Figure 2A) and similar stem loops (Supplementary Figure S3D-F). Interestingly, the highest affinity measured was for a stem loop derived from the Dengue virus subgenomic RNA (DENV-SL) that binds TRIM25 CC-PRY/SPRY with a K_D of 15.2 ± 3.0 nM (Table 1, Supplementary Figure 3). Also, TRIM25 CC-PRY/SPRY binds one of the stem loops of the reported target long-noncoding RNA (lncRNA) Lnczc3h7a with a K_D of 486 ± 77 nM (27). For pre-let-7 and to a lesser extent for the other stem loops we observed a complex binding isotherm suggesting the presence of several binding sites and a complex binding mode (Supplementary Figure S3A). Due to these complications we could only quantify and compare the highest affinity binding event. The significance of the lower affinity binding events is not clear, but since they generally feature low N-values, they may represent RNA-induced oligomerisation. This is supported by the observation of protein aggregation upon RNA addition for most of these RNAs. Filter-binding assays confirmed the stronger binding of DENV-SL compared to pre-let-7 and showed binding with nanomolar affinity also for a stem loop of *Drosophila* lncRNA roX2 (Table 2). The latter is not a reported TRIM25 target but involved in *Drosophila* dosage compensation (43) and could therefore be considered structurally and functionally unrelated, further supporting that TRIM25 binds a variety of stem-loop RNAs regardless of sequence. Affinities measured by filter-binding assays were generally higher than those by ITC, possibly because filter binding is more sensitive to aggregation.

As reported previously, we found that the affinity of the PRY/SPRY domain for pre-let-7 RNA (5.0±1.2 µM, as measured by ITC, Table 2, Figure 2B) is much weaker than for CC-PRY/SPRY (25,26). The RNA-binding of the PRY/SPRY domain alone is therefore not sufficient to explain the high affinity binding of TRIM25. The complex binding isotherm suggests that an additional binding site might be necessary for high affinity binding (Supplementary Figure S3A). This is also supported by the observation that the strong increase of affinity in the presence of the CC domain and linker region is observed for longer RNAs, but not for shorter pre-let-7 stem-only and loop-only, which show weaker binding, comparable to the PRY/SPRY alone, that can be explained by a single binding site model (Table 1, Supplementary Figure 3B and C). Sanchez *et al.* (26) described a lysine-rich stretch in the L2 linker connecting the CC and PRY/SPRY domains as necessary for binding of double-stranded RNA. Mutation of these lysines to alanine (381-392 7KA) reduced the affinity to double-stranded RNA

20-fold in the original study (26). However, in our experiments this mutant had a much weaker effect on the binding of short stem loop RNAs to CC-PRY/SPRY ($K_{D\ =}$ 428 ± 55 nM, Supplementary Figure 3L) than the original study described for binding of double stranded RNA, making it unlikely that this binding site alone is responsible for the observed increase in affinity.

Cooperative binding of PRY/SPRY and CC domain to RNA induces conformational change in TRIM25

We noted that in the crystal structure of the CC-PRY/SPRY dimer (PDB:6FLN) binding-site-1 is part of a larger positively charged surface that extends onto the CC (Figure 2B). Together, the PRY/SPRY domain and CC seem to form a joint interaction surface that could explain the tighter binding of RNA as observed by ITC and filter binding assays. The CC is not suitable for NMR studies due to its size and extended conformation, which causes slow molecular tumbling and NMR resonance line broadening beyond detection. Instead, to test the CC's putative RNA-binding capacity (12,44), we used ITC to characterize its RNA binding properties (Table 1). We found that the CC binds pre-let-7 with low micromolar affinity (8.1 ± 3.1µM) (Figure 2A), slightly weaker than the PRY/SPRY domain. For both the PRY/SPRY and the CC domain, we observed low N-values, likely indicating, that each RNA molecule is big enough to bind several domains, allowing for cooperativity. It is therefore possible that cooperative RNA-binding of the CC and PRY/SPRY domain depends on the interaction between these domains in solution. As we have previously shown, the CC: PRY/SPRY interaction is much weaker than the interaction with RNA (28). We therefore used solution small-angle X-ray scattering (SAXS) to test for a stabilisation of the transient interaction between CC and PRY/SPRY domain through RNA-binding. A comparison of the SAXS curves of free TRIM25 CC-PRY/SPRY and the complex with pre-let-7 shows a significant decrease in the radius of gyration upon RNA-binding (Rg = 6.83 ± 0.05 nm for the free protein compared to Rg = 5.69 ± 0.02 nm for the complex), indicating that the complex adopts a more compact conformation than the free protein in solution (Figure 2C), where the PRY/SPRY domain is mostly detached from the CC domain (28). This is also evident from the pairwise distance distribution, P(r), obtained from the SAXS data, where the free protein shows a broad distribution with two distinct maxima, indicating that the two domains tumble independently. In contrast, the complex shows a single maximum with a much narrower distribution, indicating that it tumbles as a single, compact entity (Figure 2C). We conclude that RNA binding enhances the interaction between the CC and PRY/SPRY domains and leads to a more compact conformation of the protein.

Mutational analysis confirms RNA-binding sites on PRY/SPRY and CC

To better understand the relative contributions of the PRY/SPRY RNA binding sites identified by NMR, and the binding site on the CC, inferred from the crystal structure of CC-PRY/SPRY (Figure 2B), we created point mutants and tested their effect on RNA binding using ITC (Table 1, Supplementary Figure S3F-L). Mutation of binding-site-1 residues (H505E/K508E) in the context of the CC-PRY/SPRY construct lead to a 6-fold reduction of affinity to pre-let-7 compared to the WT (K_D = 484 ± 48 nM). On binding-site-2, Y601 and K602 show the strongest CSPs and a K602E mutant reduced

binding by a factor of 2.5 (K_D = 196 ± 22 nM). Combination of these mutants (H505E/K508E/K602E triple-mutant) further reduces RNA-binding more than ten-fold compared to wildtype (K_D = 790 ± 160 nM). This suggests that both binding sites on the PRY/SPRY domain are critical for cooperative binding. The effect of these mutants is however not as strong as that of previously published, less conservative deletions or mutating entire regions (25,26).

The design of CC mutants turned out to be more difficult as we could only rely on indirect information in the absence of NMR data and thus inferred RNA binding residues from amino acids which are surface-exposed, close to the PRY/SPRY-CC interface and belong to typical RNA-binding residues like lysines, arginines and aromatic residues. We found that a double mutant on the basic surface close to the PRY/SPRY binding site (K283A/K285A) in the context of the CC-PRY/SPRY reduced RNA-binding about 8-fold (K_D = 606 ± 124 nM, Figure 2D). This surface patch also harbours tyrosine 278, whose phosphorylation was previously shown to affect TRIM25's E3 ligase activity (45). Since the close proximity to the RNA binding residues might suggest that phosphorylation of Y278 could also affect RNA binding, we tested RNA binding of the Y278A mutant in ITC, but found no effect on binding affinity to pre-let-7. It is however likely that additional residues on the CC are involved in RNA binding, since we restricted mutations to the proximity of the PRY/SPRY-binding site. Combination of the mutants on the CC and PRY/SPRY results in a penta-mutant that reduces binding to pre-let-7 almost 20-fold (K_D = 1.32 ± 0.37 µM). Interestingly, the double mutant Y463S/Y476S, that reduces the interaction between CC and PRY/SPRY (28) reduced also RNA binding (K_D = 252 ± 61 nM), further supporting our hypothesis in which RNA binding stabilizes the CC-PRY/SPRY interaction.

RNA binding regulates ubiquitination activity

We have previously demonstrated the importance of the transient CC-PRY/SPRY interaction for the catalytic activity of TRIM25 in RIG-I signaling (28) and as we propose a stabilization of this interaction upon RNA binding, we next investigated the effect of RNA binding mutants on the ubiquitination activity of TRIM25. To do so, we co-transfected HEK293T cells with wildtype or mutant TRIM25 and FLAG-tagged RIG-I CARDs (Figure 3A). Expression levels of TRIM25 and ubiquitination of the CARD domains were detected by Western blotting. Overexpression of wildtype TRIM25 caused robust ubiquitination of the RIG-I CARDs. However, both K602E and H505E/K508E on the PRY/SPRY as well as K283A/K285A on the CC reduced ubiquitination below the background level observed in the absence of exogenous TRIM25 expression, demonstrating that reduced RNA binding also reduces ubiquitination of RIG-I CARDs (Figure 3B). It is noteworthy that the effect of both wildtype and mutants is strongest for di- and tri-ubiquitination, while mono-ubiquitination is almost unaffected. It is possible that mono-ubiquitination of CARDs is caused by an E3 ligase other than TRIM25 or RNA binding might be required for chain elongation, but not initiation. The latter could be an E2 specific effect, supported by the observation reported earlier that Ubc13/Uev1A, the E2 complex specific for the production of K63-linked ubiquitin chains *in vitro* only produces unanchored ubiquitin chains, suggesting that a second E2 is necessary for chain initiation (46,47).

This effect is even more striking, given that mutants H505E/K508E and K602E on the PRY/SPRY, but not K283/285A on the CC, showed consistently elevated expression levels compared to the wildtype. This was confirmed by monitoring expression levels over time. Proteasome inhibition using Carfilzomib stabilized both wildtype and H505E/K508E/K602E triple mutant TRIM25, but had a much more dramatic effect on the wildtype, leading to similar expression levels than the mutant (Figure 3C). This points towards a crucial role of TRIM25-RNA binding not only in RIG-I ubiquitination but also in auto-ubiquitination of TRIM25. While in RIG-I ubiquitination TRIM25 specifically produces K63-linked chains, that do not promote proteasomal degradation, for other targets such as MAVS, ZAP or 14-3-3σ degradative K48-linked ubiquitination by TRIM25 was reported and is therefore possibly also occurring during auto-ubiquitination (16,48,49). As the RNA binding deficient mutants include the replacement of lysines, it is possible that this removes the auto-ubiquitination target lysine of TRIM25. Together with the strong reduction in substrate ubiquitination, this suggests that RNA binding enhances auto-ubiquitination of TRIM25 in cells and thereby regulates its proteasomal degradation and protein levels.

RNA-induced liquid-liquid phase separation facilitates the interaction of TRIM25 and RIG-I *in vitro*

To gain further insight into the structurally so far uncharacterized interaction of TRIM25 and RIG-I, we attempted to use NMR to map the interaction site and determine the affinity. Previous studies have established that the TRIM25 PRY/SPRY domain and the RIG-I CARDs alone are sufficient for robust interaction and ubiquitination in cells (15) (42). We therefore titrated unlabelled RIG-I CARDs into ^{15}N-labelled TRIM25 PRY/SPRY to monitor expected chemical shift perturbations and/or line broadening to identify interacting residues. However, while such an approach would almost certainly detect any direct interaction with affinities down to low millimolar affinities, we did not observe any signs of interaction (Figure 4A). While not completely ruling out the possibility of a TRIM25-RIG-I interaction, this strongly suggests the absence of a direct interaction between TRIM25 PRY/SPRY and RIG-I CARDs. D'Cruz *et al.* (42) proposed a mechanism of RIG-I binding, that would involve displacement of the N-terminal helix α1 of the PRY/SPRY by a similar helix in the CARDs. We therefore characterized secondary structure and flexibility of α1 using ^{15}N relaxation measurements and heteronuclear NOEs (HetNOE). We found that α1 forms a stable helix in solution and tumbles together with the core domain, as residues in this region have the same apparent rotational correlation time as the entire domain. This indicates that a mechanism that involves unfolding or flipping out of α1 is very unlikely (Figure 4B-D) and agrees with earlier observations, that although the functional interaction between TRIM25 and RIG-I is very well established in cells, there is no evidence for their direct interaction *in vitro (26)*. Several additional factors thought to stabilize the interaction, including both proteins and RNAs, have been proposed (27,44,50).

Since we observed a significant overlap of mutants previously described to reduce TRIM25/RIG-I interaction (42) with our binding-site-2, that is specific to double-stranded RNA, we set out to further investigate the possible stabilization of the TRIM25/RIG-I interaction by RNA.

We transfected HeLa cells with mEGFP-fused TRIM25 and dTomato-fused CARDs and performed live cell imaging. In most cells, both TRIM25 and RIG-I showed a diffuse distribution in the cytoplasm with some cells showing enrichment of TRIM25 in cytoplasmic granules (Supplementary Figure S4). Upon induction of stress using sodium arsenite, TRIM25 relocalized to smaller, well defined puncta in the cytosol that in a few cases also contained RIG-I CARDs. This confirms previous research showing that both TRIM25 and RIG-I are constituents of stress granules, a membrane-less organelle formed by liquid-liquid phase separation around mRNAs (26,51-53). In comparison, the H505E/K508/K602E RNA-binding deficient mutant showed a stronger localization to granules in the nucleus and its vicinity. It is however not clear if this re-localization is a consequence of reduced RNA-binding, auto-ubiquitination or increased expression levels of this mutant. Nuclear TRIM25 has been previously reported, but its significance remains unclear (54). In summary, this shows that TRIM25 can be part of various cytoplasmic and nuclear granules, although this commonly requires a stimulus such as oxidative stress.

Interestingly, we observed similar liquid-liquid phase separation of TRIM25 CC-PRY/SPRY in the presence of the DENV-SL RNA *in vitro* (Figure 5A). Liquid-liquid phase separation in low salt (100 µM) occurred at equimolar concentrations of protein and RNA down to 1 µM. Phase-separation of the protein or RNA alone was not observed at concentrations up to at least 400 µM. Interestingly, all other RNAs investigated in this study did not promote the formation of macromolecular condensates *in vitro*. Due to the very high affinity of the DENV-SL RNA (15.2 ± 3.0 nM) even the penta-mutant K283A/K285A/H505E/K508E/K602E, that reduced binding to pre-let-7 20-fold, did not impair phase-separation at concentrations down to 1µM. Intriguingly, RFP-fused RIG-I CARDs enriched more than 20-fold in these droplets, while only less than two-fold enrichment of RFP alone was observed (Figure 5B). This is remarkable, since CARDs have no known RNA-binding activity (27,55). To our knowledge this is the first evidence for an interaction between TRIM25 and RIG-I *in vitro*, although it is at this stage not clear if this is due to direct protein/protein interactions or so far unobserved RNA-binding of RIG-I CARDs. However, our NMR experiments rule out a direct PRY/SPRY:RIG-I CARDs interaction unless RNA binding of the PRY/SPRY allosterically increases affinity to CARDs. The observation that the T55I mutation on the CARDs, that was reported to reduce TRIM25/RIG-I interaction in cells, has no such effect in our *in vitro* assays further shows that a binary PRY/SPRY:CARDs interaction is insufficient to explain the association (2). Irrespective of the nature of this interaction, this experiment demonstrates that RNA-induced liquid-liquid phase separation could account for the efficient recruitment of RIG-I to TRIM25 despite the absence of detectable interactions between the isolated proteins. The described system might therefore act as a model system to further study the determinants of liquid-liquid phase separation and RIG-I activation by TRIM25.

DISCUSSION

In summary, we show that TRIM25 achieves very tight binding of RNA through several binding sites on the CC and PRY/SPRY domain, with each binding site showing only weak affinities to RNA and different specificities. While we confirm and refine a previously identified binding region on the PRY/SPRY, we found additional binding sites on the PRY/SPRY and CC. The novel second binding

site on the PRY/SPRY seems to be specific for double-stranded RNA and overlaps with a region previously thought to be involved in RIG-I binding (42). The close proximity of binding sites specific for single and double stranded RNA suggests a specificity for structure rather than sequence and indeed we found binding with nanomolar affinity to several stem-loops regardless of sequence. This may explain the failure of previous studies to identify a clear RNA motif for TRIM25 (23). The highly cooperative binding mode involving multiple binding sites on different domains is critical for the E3-ubiquitin ligase activity of TRIM25, as RNA binding stabilizes the weak interaction between the CC and PRY/SPRY domain which was previously shown to be critical for TRIM25's catalytic activity (28). In the absence of structural data of the complete tripartite motif of TRIM25 the importance of this interaction can be understood by considering two recently published structures of the tripartite motif of TRIM28, a distant relative of TRIM25 (56,57) (Figure 6). These structures show that the RING domain binds the CC at a position close to the binding site of the PRY/SPRY domain in TRIM25 (Figure 6A). RNA-mediated binding of the PRY/SPRY domain to the CC will therefore bring the PRY/SPRY domain and any substrate bound by it in close proximity to the RING domain and the bound and ubiquitin-loaded E2 conjugating enzyme, facilitating substrate ubiquitination. This is in accordance with the finding of us and others, that TRIM25 RNA-binding is required for efficient ubiquitination of the RIG-I CARDs (26). It is however not clear how RING dimerization, that is necessary for the E3 ligase activity of TRIM25 but not TRIM28, is achieved in this model (46,47,58). Such RING dimerization could occur between two TRIM25 dimers stacking up end to end. Such an inter-dimer association could also be facilitated by RNA binding, especially through enrichment in RNA granules leading to high concentrations. Alternative models have been proposed, that place the RING domain closer to the center of the CC, allowing for RING dimerization within the TRIM25 dimer (47,59)

We note that our proposed mechanism of TRIM25 activation resembles the mechanism of RNA dependent regulation of the E3-ubiquitin ligase activity of roquins (60): Roquins feature two rigid multi-domain motifs, that are connected by a flexible linker and both bind RNA. RNA binding therefore removes flexibility from the system and forces the protein into an active conformation. It should be noted, that in this case the effect is E2 dependent, so that RNA binding not only changes the extent of ubiquitination, but also specificity for certain chain compositions. Similar effects might also occur for TRIM25, as the close proximity of the RNA binding site and the RING domain in the above model combined with the necessity to accommodate both RNA and the E2~ubiquitin conjugate likely cause steric restrictions for the full complex. Such an interference of the RING domain with RNA binding could explain the earlier observation that RNA binding of full-length TRIM25 is weaker than that of CC-SPRY alone (26).

In vitro liquid-liquid phase separation of TRIM25 upon RNA binding possibly explains TRIM25's previously observed subcellular localisation in RNA-granules upon overexpression or viral stress (7,26). Liquid-liquid phase-separated macromolecular condensates allow for free diffusion of moderately large molecules, including proteins, and exchange with the surrounding liquid while at the same time featuring very high protein concentrations and frequent encounters between proteins (61). In contrast to other previously observed mechanisms of oligomerisation in TRIM proteins, the RNA-

induced liquid-liquid phase separation of TRIM25 does not require the B-Boxes, but the presence of the CC and PRY/SPRY domains is sufficient. This suggests possible mechanisms in which either more than one TRIM25 dimer can bind to one RNA molecule leading to a linear polymer or the PRY/SPRY domains of one TRIM25 molecule binds to the CC of a different molecule, an interaction that is strongly enhanced by RNA binding and could ultimately lead to formation of a cross-linked gel (Figure 6B). The necessity for binding of more than one TRIM25 dimer might explain why DENV-SL, but not the smaller pre-let-7 or lnczc3h7a stem loops induce phase separation. In this case, it should be expected that in the cellular context with RNA targets much longer than the minimal constructs used in this study, formation of TRIM25-RNA macromolecular condensates should be a common occurrence. Sanchez et al. noted that phase-separated condensates might form the necessary environment allowing for efficient interaction between TRIM25 and RIG-I and thereby resolve the apparent paradox that the TRIM25/RIG-I interaction is well established *in vivo*, but could not be reconstituted *in vitro* (26).

Indeed, we found no evidence for a direct interaction between the TRIM25 PRY/SPRY and RIG-I CARDs in our NMR experiments, although these two domains alone are sufficient for co-immunoprecipitation from cells (15). We noted however, that several of the mutants described to reduce the interaction between TRIM25 and RIG-I (F592, I594, L604 in murine TRIM25, corresponding to F597, I589 and L599 in human TRIM25) are located on or close to the second RNA binding site on the PRY/SPRY domain (42). This suggests that RNA binding of both proteins to double-stranded segments in the same RNA could play a crucial role in RIG-I activation (Figure 7). This finding is supported by the recent identification of long non-coding RNAs that bind to both TRIM25 and RIG-I and facilitate their interaction (27,44). One of these RNAs is lnczc3h7a, that was described to interact with the RIG-I helicase domain independently of viral RNA and does not release autoinhibition of RIG-I (27). However, this cannot explain how isolated RIG-I CARDs *in vitro* enrich in TRIM25/DENV-SL droplets, which requires either so far unreported RNA binding of the CARDs, an unreported interaction between CARDs and TRIM25 CC rather than PRY/SPRY or an allosteric change in TRIM25 upon RNA binding leading to increased affinity to CARDs.

Considering these new findings, we propose a mechanism, in which RNA-binding of TRIM25 not only assists in the recruitment of RIG-I through binding to the same RNA molecule or localization to phase-separated condensates, but also directly activates the E3-ubiquitin ligase activity of TRIM25 by facilitating the interaction of the PRY/SPRY and CC domains (Figure 7). Like RIG-I, many other substrates of TRIM25, e.g. ZAP, TUT4, MDM2 and p53 (23,24,49,62,63), are putative RNA binding proteins and a mechanism that involves recruitment of these substrates through binding to the same RNA molecule or enrichment in RNA granules and activation of the TRIM25 E3 ligase activity through RNA-binding might be more universal.

Several E3 ligases other than TRIM25 promote ubiquitination of RIG-I leading to controversial discussions about their relative importance (64-69). Among these are several TRIM proteins (TRIM4, 15, 40) and Riplet, a close relative of TRIM25, that lost the B-Box domains and parts of the CC (70-72). Mechanistically, a sequential ubiquitination of RIG-I by first Riplet in the CTD and then TRIM25 at

the CARDs has been proposed (68). It is noteworthy that although Riplet is closely related to TRIM25, it has lost the regions on the CC and in the L2 linker, which harbors RNA binding in TRIM25, and the RNA binding lysines and histidine found in the PRY/SPRY are not conserved. Interestingly, while the RNA-binding interface of TRIM25 is not conserved in Riplet at least one other E3 ligase ubiquitinating RIG-I, MEX3C, is an RBP (64), suggesting that a role of RNA-binding in substrate recruitment might be more common in other E3 ligases.

Despite the clear evidence for an activating role of RNA in RIG-I signaling, the role of Dengue virus subgenomic RNA in inhibition of interferon expression remains unexplained (3). We found that TRIM25 binds a stem-loop of the Dengue virus subgenomic RNA with almost ten-fold higher affinity than the TRIM25-binding stem-loop of lnczc3h7a, a long non-coding RNA that binds both TRIM25 and RIG-I and thereby facilitates interferon expression (27). This suggests that the subgenomic RNA can outcompete lnczc3h7a for TRIM25 binding. It is however not clear what the effect of this competition is, since in our *in vitro* experiments the DENV-SL RNA still promoted association of TRIM25 and RIG-I. This agrees with the original reports which found that the viral subgenomic RNA did not reduce TRIM25/RIG-I co-purification (3). A possible explanation might be that rather than inhibiting the ubiquitination of RIG-I, it could prevent the re-localization of TRIM25/RIG-I complexes to the mitochondrial membrane and thereby downstream activation of MAVS (73) by targeting them to RNA granules as we observed *in vitro*. RNA binding might also play a key role in other viral inhibition mechanisms for TRIM25. Most notably, the Influenza A non-structural protein 1 (NS1) also features an RNA-binding domain in addition to the TRIM25 binding effector domain (ED) (2,28). Interestingly, *in vitro* the ED alone is sufficient to explain binding to TRIM25, but in cells co-purification with TRIM25 depends on the presence of both domains (2,28). This suggests that binding to the same RNA could also stabilize the TRIM25/NS1 interaction, thus deactivating TRIM25-mediated ubiquitination. A similar mechanism was recently proposed for the interaction of NS1 with DHX30 (74). The inhibition of TRIM25 by other viral proteins such as paramyxovirus protein V and coronavirus protein N even depends only on their C-terminal domains that are also RBDs (4,7,75,76). RNA binding might therefore be widely exploited by viruses to inhibit TRIM25 and its crucial function in innate immunity.

ACCESSION NUMBERS

Backbone assignments of the TRIM25-PRY/SPRY domain and extended PRY/SPRY domain have been deposited at the Biological Magnetic Resonance Bank (BMRB) under accession codes 27381 and 50226.

ACKNOWLEDGEMENT

We thank the ESRF Grenoble (beamline BM29), EMBL/DESY Hamburg PETRA-III (P12 beamline), and the ILL (D22 beamline) local contacts for support (Taisiia Cheremnykh, Andrey Gruzinov, Al Kikhney, Gabriele Giachin and Anne Martel). We also thank Lucía Alvarez for critical reading of the manuscript. This work was supported by the Francis Crick Institute which receives its core funding

from Cancer Research UK (FC001142 to K.R.), the UK Medical Research Council (FC001142 to K.R.) and the Wellcome Trust (FC001142 to K.R.). J.H. gratefully acknowledges support via an Emmy-Noether Fellowship (HE 7291_1) and the Priority Program SPP1935 of the Deutsche Forschungsgemeinschaft (DFG) and the EMBL.

FUNDING

This work was supported by the Francis Crick Institute which receives its core funding from Cancer Research UK (FC001142 to K.R.), the UK Medical Research Council (FC001142 to K.R.) and the Wellcome Trust (FC001142 to K.R.) and an Emmy-Noether Fellowship and a priority program to J.H., the Deutsche Forschungsgemeinschaft (DFG) [HE 7291_1, Priority Program SPP1935 to J.H.]).

CONFLICT OF INTEREST

The authors declare no competing interests.

REFERENCES

1. Kell, A.M. and Gale, M., Jr. (2015) RIG-I in RNA virus recognition. *Virology*, **479-480**, 110-121.
2. Gack, M.U., Albrecht, R.A., Urano, T., Inn, K.-S., Huang, I.C., Carnero, E., Farzan, M., Inoue, S., Jung, J.U. and García-Sastre, A. (2009) Influenza A virus NS1 targets the ubiquitin ligase TRIM25 to evade recognition by the host viral RNA sensor RIG-I. *Cell Host Microbe*, **5**, 439-449.
3. Manokaran, G., Finol, E., Wang, C., Gunaratne, J., Bahl, J., Ong, E.Z., Tan, H.C., Sessions, O.M., Ward, A.M., Gubler, D.J. *et al.* (2015) Dengue subgenomic RNA binds TRIM25 to inhibit interferon expression for epidemiological fitness. *Science*, **350**, 217-221.
4. Hu, Y., Li, W., Gao, T., Cui, Y., Jin, Y., Li, P., Ma, Q., Liu, X. and Cao, C. (2017) The Severe Acute Respiratory Syndrome Coronavirus Nucleocapsid Inhibits Type I Interferon Production by Interfering with TRIM25-Mediated RIG-I Ubiquitination. *Journal of Virology*, **91**, e02143-02116.
5. Gupta, S., Ylä-Anttila, P., Callegari, S., Tsai, M.-H., Delecluse, H.-J. and Masucci, M.G. (2018) Herpesvirus deconjugases inhibit the IFN response by promoting TRIM25 autoubiquitination and functional inactivation of the RIG-I signalosome. *PLOS Pathogens*, **14**, e1006852.
6. Castello, A., Fischer, B., Frese, C.K., Horos, R., Alleaume, A.-M., Foehr, S., Curk, T., Krijgsveld, J. and Hentze, M.W. (2016) Comprehensive Identification of RNA-Binding Domains in Human Cells. *Mol Cell*, **63**, 696-710.
7. Sánchez-Aparicio, M.T., Feinman, L.J., García-Sastre, A. and Shaw, M.L. (2018) Paramyxovirus V Proteins Interact with the RIG-I/TRIM25 Regulatory Complex and Inhibit RIG-I Signaling. *Journal of Virology*, **92**, e01960-01917.
8. Coltart, C.E.M., Lindsey, B., Ghinai, I., Johnson, A.M. and Heymann, D.L. (2017) The Ebola outbreak, 2013-2016: old lessons for new epidemics. *Philos Trans R Soc Lond B Biol Sci*, **372**, 20160297.

9. Li, J.-Y., You, Z., Wang, Q., Zhou, Z.-J., Qiu, Y., Luo, R. and Ge, X.-Y. (2020) The epidemic of 2019-novel-coronavirus (2019-nCoV) pneumonia and insights for emerging infectious diseases in the future. *Microbes Infect*, **22**, 80-85.
10. Ebi, K.L. and Nealon, J. (2016) Dengue in a changing climate. *Environmental Research*, **151**, 115-123.
11. Krammer, F., Smith, G.J.D., Fouchier, R.A.M., Peiris, M., Kedzierska, K., Doherty, P.C., Palese, P., Shaw, M.L., Treanor, J., Webster, R.G. *et al.* (2018) Influenza. *Nat Rev Dis Primers*, **4**, 3-3.
12. Kwon, S.C., Yi, H., Eichelbaum, K., Föhr, S., Fischer, B., You, K.T., Castello, A., Krijgsveld, J., Hentze, M.W. and Kim, V.N. (2013) The RNA-binding protein repertoire of embryonic stem cells. *Nature Structural & Molecular Biology*, **20**, 1122-1130.
13. Williams Felix, P., Haubrich, K., Perez-Borrajero, C. and Hennig, J. (2019), *Biological Chemistry*, Vol. 400, pp. 1443.
14. Sardiello, M., Cairo, S., Fontanella, B., Ballabio, A. and Meroni, G. (2008) Genomic analysis of the TRIM family reveals two groups of genes with distinct evolutionary properties. *BMC Evolutionary Biology*, **8**, 225.
15. Gack, M.U., Shin, Y.C., Joo, C.-H., Urano, T., Liang, C., Sun, L., Takeuchi, O., Akira, S., Chen, Z., Inoue, S. *et al.* (2007) TRIM25 RING-finger E3 ubiquitin ligase is essential for RIG-I-mediated antiviral activity. *Nature*, **446**, 916-920.
16. Castanier, C., Zemirli, N., Portier, A., Garcin, D., Bidère, N., Vazquez, A. and Arnoult, D. (2012) MAVS ubiquitination by the E3 ligase TRIM25 and degradation by the proteasome is involved in type I interferon production after activation of the antiviral RIG-I-like receptors. *BMC Biology*, **10**, 44.
17. Orimo, A., Inoue, S., Minowa, O., Tominaga, N., Tomioka, Y., Sato, M., Kuno, J., Hiroi, H., Shimizu, Y., Suzuki, M. *et al.* (1999) Underdeveloped uterus and reduced estrogen responsiveness in mice with disruption of the estrogen-responsive finger protein gene, which is a direct target of estrogen receptor α. *Proceedings of the National Academy of Sciences*, **96**, 12027-12032.
18. Qin, Y., Cui, H. and Zhang, H. (2016) Overexpression of TRIM25 in Lung Cancer Regulates Tumor Cell Progression. *Technology in Cancer Research & Treatment*, **15**, 707-715.
19. Takayama, K.-i., Suzuki, T., Tanaka, T., Fujimura, T., Takahashi, S., Urano, T., Ikeda, K. and Inoue, S. (2018) TRIM25 enhances cell growth and cell survival by modulating p53 signals via interaction with G3BP2 in prostate cancer. *Oncogene*, **37**, 2165-2180.
20. Luo, D., Ding, Steve C., Vela, A., Kohlway, A., Lindenbach, Brett D. and Pyle, Anna M. (2011) Structural Insights into RNA Recognition by RIG-I. *Cell*, **147**, 409-422.
21. Kolakofsky, D., Kowalinski, E. and Cusack, S. (2012) A structure-based model of RIG-I activation. *RNA*, **18**, 2118-2127.
22. Ren, X., Linehan, M.M., Iwasaki, A. and Pyle, A.M. (2019) RIG-I Selectively Discriminates against 5′-Monophosphate RNA. *Cell Rep*, **26**, 2019-2027.e2014.
23. Choudhury, N.R., Nowak, J.S., Zuo, J., Rappsilber, J., Spoel, S.H. and Michlewski, G. (2014) Trim25 Is an RNA-Specific Activator of Lin28a/TuT4-Mediated Uridylation. *Cell Rep*, **9**, 1265-1272.
24. Zheng, X., Wang, X., Tu, F., Wang, Q., Fan, Z. and Gao, G. (2017) TRIM25 Is Required for the Antiviral Activity of Zinc Finger Antiviral Protein. *Journal of Virology*, **91**, e00088-00017.
25. Choudhury, N.R., Heikel, G., Trubitsyna, M., Kubik, P., Nowak, J.S., Webb, S., Granneman, S., Spanos, C., Rappsilber, J., Castello, A. *et al.* (2017) RNA-binding activity of TRIM25 is mediated by its PRY/SPRY domain and is required for ubiquitination. *BMC Biology*, **15**, 105.
26. Sanchez, J.G., Sparrer, K.M.J., Chiang, C., Reis, R.A., Chiang, J.J., Zurenski, M.A., Wan, Y., Gack, M.U. and Pornillos, O. (2018) TRIM25 Binds RNA to Modulate Cellular Anti-viral Defense. *Journal of Molecular Biology*, **430**, 5280-5293.
27. Lin, H., Jiang, M., Liu, L., Yang, Z., Ma, Z., Liu, S., Ma, Y., Zhang, L. and Cao, X. (2019) The long noncoding RNA Lnczc3h7a promotes a TRIM25-mediated RIG-I antiviral innate immune response. *Nature Immunology*, **20**, 812-823.
28. Koliopoulos, M.G., Lethier, M., van der Veen, A.G., Haubrich, K., Hennig, J., Kowalinski, E., Stevens, R.V., Martin, S.R., Reis e Sousa, C., Cusack, S. *et al.* (2018) Molecular mechanism of influenza A NS1-mediated TRIM25 recognition and inhibition. *Nature Communications*, **9**, 1820.
29. de Marco, A., Deuerling, E., Mogk, A., Tomoyasu, T. and Bukau, B. (2007) Chaperone-based procedure to increase yields of soluble recombinant proteins produced in E. coli. *BMC Biotechnol*, **7**, 32-32.

30. Delaglio, F., Grzesiek, S., Vuister, G.W., Zhu, G., Pfeifer, J. and Bax, A. (1995) NMRPipe: A multidimensional spectral processing system based on UNIX pipes. *Journal of Biomolecular NMR*, **6**, 277-293.
31. Lee, W., Tonelli, M. and Markley, J.L. (2014) NMRFAM-SPARKY: enhanced software for biomolecular NMR spectroscopy. *Bioinformatics*, **31**, 1325-1327.
32. Shen, Y., Delaglio, F., Cornilescu, G. and Bax, A. (2009) TALOS+: a hybrid method for predicting protein backbone torsion angles from NMR chemical shifts. *Journal of Biomolecular NMR*, **44**, 213-223.
33. Shen, Y. and Bax, A. (2010) SPARTA+: a modest improvement in empirical NMR chemical shift prediction by means of an artificial neural network. *Journal of Biomolecular NMR*, **48**, 13-22.
34. Niklasson, M., Otten, R., Ahlner, A., Andresen, C., Schlagnitweit, J., Petzold, K. and Lundström, P. (2017) Comprehensive analysis of NMR data using advanced line shape fitting. *Journal of Biomolecular NMR*, **69**, 93-99.
35. Kay, L.E., Torchia, D.A. and Bax, A. (1989) Backbone dynamics of proteins as studied by nitrogen-15 inverse detected heteronuclear NMR spectroscopy: application to staphylococcal nuclease. *Biochemistry*, **28**, 8972-8979.
36. Zhu, G., Xia, Y., Nicholson, L.K. and Sze, K.H. (2000) Protein Dynamics Measurements by TROSY-Based NMR Experiments. *Journal of Magnetic Resonance*, **143**, 423-426.
37. Blanchet, C.E., Spilotros, A., Schwemmer, F., Graewert, M.A., Kikhney, A., Jeffries, C.M., Franke, D., Mark, D., Zengerle, R., Cipriani, F. *et al.* (2015) Versatile sample environments and automation for biological solution X-ray scattering experiments at the P12 beamline (PETRA III, DESY). *Journal of Applied Crystallography*, **48**, 431-443.
38. Franke, D., Petoukhov, M.V., Konarev, P.V., Panjkovich, A., Tuukkanen, A., Mertens, H.D.T., Kikhney, A.G., Hajizadeh, N.R., Franklin, J.M., Jeffries, C.M. *et al.* (2017) ATSAS 2.8: a comprehensive data analysis suite for small-angle scattering from macromolecular solutions. *Journal of Applied Crystallography*, **50**, 1212-1225.
39. Konarev, P.V., Volkov, V.V., Sokolova, A.V., Koch, M.H.J. and Svergun, D.I. (2003) PRIMUS: a Windows PC-based system for small-angle scattering data analysis. *Journal of Applied Crystallography*, **36**, 1277-1282.
40. Svergun, D. (1992) Determination of the regularization parameter in indirect-transform methods using perceptual criteria. *Journal of Applied Crystallography*, **25**, 495-503.
41. Schindelin, J., Arganda-Carreras, I., Frise, E., Kaynig, V., Longair, M., Pietzsch, T., Preibisch, S., Rueden, C., Saalfeld, S., Schmid, B. *et al.* (2012) Fiji: an open-source platform for biological-image analysis. *Nature Methods*, **9**, 676-682.
42. D'Cruz, A.A., Kershaw, N.J., Hayman, T.J., Linossi, E.M., Chiang, J.J., Wang, M.K., Dagley, L.F., Kolesnik, T.B., Zhang, J.-G., Masters, S.L. *et al.* (2018) Identification of a second binding site on the TRIM25 B30.2 domain. *Biochemical Journal*, **475**, 429-440.
43. Meller, V.H. and Rattner, B.P. (2002) The roX genes encode redundant male-specific lethal transcripts required for targeting of the MSL complex. *EMBO J*, **21**, 1084-1091.
44. Lai, C., Liu, L., Liu, Q., Cheng, S., Wang, K., Zhao, L., Xia, M., Wang, C., Gu, H., Duan, Y. *et al.* (2019) Long noncoding RNA AVAN promotes antiviral innate immunity by interacting with TRIM25 and enhancing the transcription of FOXO3a. *bioRxiv*, 623132.
45. Lee, N.-R., Choi, J.-Y., Yoon, I.-H., Lee, J.K. and Inn, K.-S. (2018) Positive regulatory role of c-Src-mediated TRIM25 tyrosine phosphorylation on RIG-I ubiquitination and RIG-I-mediated antiviral signaling pathway. *Cellular Immunology*, **332**, 94-100.
46. Sanchez, J.G., Chiang, J.J., Sparrer, K.M.J., Alam, S.L., Chi, M., Roganowicz, M.D., Sankaran, B., Gack, M.U. and Pornillos, O. (2016) Mechanism of TRIM25 Catalytic Activation in the Antiviral RIG-I Pathway. *Cell Rep*, **16**, 1315-1325.
47. Koliopoulos, M.G., Esposito, D., Christodoulou, E., Taylor, I.A. and Rittinger, K. (2016) Functional role of TRIM E3 ligase oligomerization and regulation of catalytic activity. *EMBO J*, **35**, 1204-1218.
48. Urano, T., Saito, T., Tsukui, T., Fujita, M., Hosoi, T., Muramatsu, M., Ouchi, Y. and Inoue, S. (2002) Efp targets 14-3-3σ for proteolysis and promotes breast tumour growth. *Nature*, **417**, 871-875.
49. Li, M.M.H., Lau, Z., Cheung, P., Aguilar, E.G., Schneider, W.M., Bozzacco, L., Molina, H., Buehler, E., Takaoka, A., Rice, C.M. *et al.* (2017) TRIM25 Enhances the Antiviral Action of Zinc-Finger Antiviral Protein (ZAP). *PLOS Pathogens*, **13**, e1006145.

50. Liu, Z., Wu, C., Pan, Y., Liu, H., Wang, X., Yang, Y., Gu, M., Zhang, Y. and Wang, X. (2019) NDR2 promotes the antiviral immune response via facilitating TRIM25-mediated RIG-I activation in macrophages. *Science Advances*, **5**, eaav0163.
51. Onomoto, K., Jogi, M., Yoo, J.-S., Narita, R., Morimoto, S., Takemura, A., Sambhara, S., Kawaguchi, A., Osari, S., Nagata, K. *et al.* (2012) Critical Role of an Antiviral Stress Granule Containing RIG-I and PKR in Viral Detection and Innate Immunity. *PLOS ONE*, **7**, e43031.
52. Jain, S., Wheeler, J.R., Walters, R.W., Agrawal, A., Barsic, A. and Parker, R. (2016) ATPase-Modulated Stress Granules Contain a Diverse Proteome and Substructure. *Cell*, **164**, 487-498.
53. Markmiller, S., Soltanieh, S., Server, K.L., Mak, R., Jin, W., Fang, M.Y., Luo, E.-C., Krach, F., Yang, D., Sen, A. *et al.* (2018) Context-Dependent and Disease-Specific Diversity in Protein Interactions within Stress Granules. *Cell*, **172**, 590-604.e513.
54. Meyerson, N.R., Zhou, L., Guo, Y.R., Zhao, C., Tao, Y.J., Krug, R.M. and Sawyer, S.L. (2017) Nuclear TRIM25 Specifically Targets Influenza Virus Ribonucleoproteins to Block the Onset of RNA Chain Elongation. *Cell Host Microbe*, **22**, 627-638.e627.
55. Hornung, V., Ellegast, J., Kim, S., Brzózka, K., Jung, A., Kato, H., Poeck, H., Akira, S., Conzelmann, K.-K., Schlee, M. *et al.* (2006) 5'-Triphosphate RNA Is the Ligand for RIG-I. *Science*, **314**, 994-997.
56. Stoll, G.A., Oda, S.-i., Chong, Z.-S., Yu, M., McLaughlin, S.H. and Modis, Y. (2019) Structure of KAP1 tripartite motif identifies molecular interfaces required for retroelement silencing. *Proceedings of the National Academy of Sciences*, **116**, 15042-15051.
57. Lim, M., Newman, J.A., Williams, H.L., Masino, L., Aitkenhead, H., Gravard, A.E., Gileadi, O. and Svejstrup, J.Q. (2019) A Ubiquitin-Binding Domain that Binds a Structural Fold Distinct from that of Ubiquitin. *Structure*, **27**, 1316-1325.e1316.
58. Stevens, R.V., Esposito, D. and Rittinger, K. (2019) Characterisation of class VI TRIM RING domains: linking RING activity to C-terminal domain identity. *Life Sci Alliance*, **2**, e201900295.
59. Gupta, S., Ylä-Anttila, P., Sandalova, T., Sun, R., Achour, A. and Masucci, M.G. (2019) 14-3-3 scaffold proteins mediate the inactivation of trim25 and inhibition of the type I interferon response by herpesvirus deconjugases. *PLOS Pathogens*, **15**, e1008146.
60. Zhang, Q., Fan, L., Hou, F., Dong, A., Wang, Y.-X. and Tong, Y. (2015) New Insights into the RNA-Binding and E3 Ubiquitin Ligase Activities of Roquins. *Scientific Reports*, **5**, 15660.
61. Banani, S.F., Lee, H.O., Hyman, A.A. and Rosen, M.K. (2017) Biomolecular condensates: organizers of cellular biochemistry. *Nature Reviews Molecular Cell Biology*, **18**, 285-298.
62. Elenbaas, B., Dobbelstein, M., Roth, J., Shenk, T. and Levine, A.J. (1996) The MDM2 oncoprotein binds specifically to RNA through its RING finger domain. *Mol Med*, **2**, 439-451.
63. Riley, K.J.L. and Maher, L.J., 3rd. (2007) p53 RNA interactions: new clues in an old mystery. *RNA*, **13**, 1825-1833.
64. Kuniyoshi, K., Takeuchi, O., Pandey, S., Satoh, T., Iwasaki, H., Akira, S. and Kawai, T. (2014) Pivotal role of RNA-binding E3 ubiquitin ligase MEX3C in RIG-I–mediated antiviral innate immunity. *Proceedings of the National Academy of Sciences*, **111**, 5646-5651.
65. Gao, D., Yang, Y.-K., Wang, R.-P., Zhou, X., Diao, F.-C., Li, M.-D., Zhai, Z.-H., Jiang, Z.-F. and Chen, D.-Y. (2009) REUL Is a Novel E3 Ubiquitin Ligase and Stimulator of Retinoic-Acid-Inducible Gene-I. *PLOS ONE*, **4**, e5760.
66. Oshiumi, H., Matsumoto, M., Hatakeyama, S. and Seya, T. (2009) Riplet/RNF135, a RING Finger Protein, Ubiquitinates RIG-I to Promote Interferon-β Induction during the Early Phase of Viral Infection. *Journal of Biological Chemistry*, **284**, 807-817.
67. Hayman, T.J., Hsu, A.C., Kolesnik, T.B., Dagley, L.F., Willemsen, J., Tate, M.D., Baker, P.J., Kershaw, N.J., Kedzierski, L., Webb, A.I. *et al.* (2019) RIPLET, and not TRIM25, is required for endogenous RIG-I-dependent antiviral responses. *Immunology & Cell Biology*, **97**, 840-852.
68. Okamoto, M., Kouwaki, T., Fukushima, Y. and Oshiumi, H. (2018) Regulation of RIG-I Activation by K63-Linked Polyubiquitination. *Frontiers in Immunology*, **8**, 1942.
69. Cadena, C., Ahmad, S., Xavier, A., Willemsen, J., Park, S., Park, J.W., Oh, S.-W., Fujita, T., Hou, F., Binder, M. *et al.* (2019) Ubiquitin-Dependent and -Independent Roles of E3 Ligase RIPLET in Innate Immunity. *Cell*, **177**, 1187-1200.e1116.
70. Uchil, P.D., Hinz, A., Siegel, S., Coenen-Stass, A., Pertel, T., Luban, J. and Mothes, W. (2013) TRIM Protein-Mediated Regulation of Inflammatory and Innate Immune Signaling and Its Association with Antiretroviral Activity. *Journal of Virology*, **87**, 257-272.

71. Zhao, C., Jia, M., Song, H., Yu, Z., Wang, W., Li, Q., Zhang, L., Zhao, W. and Cao, X. (2017) The E3 Ubiquitin Ligase TRIM40 Attenuates Antiviral Immune Responses by Targeting MDA5 and RIG-I. *Cell Rep*, **21**, 1613-1623.
72. Yan, J., Li, Q., Mao, A.-P., Hu, M.-M. and Shu, H.-B. (2014) TRIM4 modulates type I interferon induction and cellular antiviral response by targeting RIG-I for K63-linked ubiquitination. *Journal of Molecular Cell Biology*, **6**, 154-163.
73. Wu, B. and Hur, S. (2015) How RIG-I like receptors activate MAVS. *Curr Opin Virol*, **12**, 91-98.
74. Chen, G., Ma, L.-C., Wang, S., Woltz, R.L., Grasso, E.M., Montelione, G.T. and Krug, R.M. (2019) A double-stranded RNA platform is required for the interaction between a host restriction factor and the NS1 protein of influenza A virus. *Nucleic Acids Research*, **48**, 304-315.
75. Hsin, W.-C., Chang, C.-H., Chang, C.-Y., Peng, W.-H., Chien, C.-L., Chang, M.-F. and Chang, S.C. (2018) Nucleocapsid protein-dependent assembly of the RNA packaging signal of Middle East respiratory syndrome coronavirus. *Journal of Biomedical Science*, **25**, 47.
76. Parks, C.L., Witko, S.E., Kotash, C., Lin, S.L., Sidhu, M.S. and Udem, S.A. (2006) Role of V protein RNA binding in inhibition of measles virus minigenome replication. *Virology*, **348**, 96-106.
77. Gack, M.U., Kirchhofer, A., Shin, Y.C., Inn, K.-S., Liang, C., Cui, S., Myong, S., Ha, T., Hopfner, K.-P. and Jung, J.U. (2008) Roles of RIG-I N-terminal tandem CARD and splice variant in TRIM25-mediated antiviral signal transduction. *Proceedings of the National Academy of Sciences*, **105**, 16743.
78. Gack, M.U., Nistal-Villán, E., Inn, K.-S., García-Sastre, A. and Jung, J.U. (2010) Phosphorylation-Mediated Negative Regulation of RIG-I Antiviral Activity. *Journal of Virology*, **84**, 3220.

TABLE AND FIGURES LEGENDS

Table 1. ITC data for various TRIM25 constructs and RNAs: Titrations with CC-PRY/SPRY constructs required fitting of a two-site model for larger RNAs. CC-PRY/SPRY and pre-let-7 showed several binding sites, of which only the highest affinity binding could be measured. The individual domains CC and PRY/SPRY show low N values, most likely explained by binding of several domains to one RNA.

protein	RNA	K_D (M)	N	ΔH (kJ/mol)
PRY/SPRY	pre-let-7-1a@2	$5.0 \pm 1.2\ 10^{-6}$	0.711 ± 0.020	-29.9 ± 1.6
CC	pre-let-7-1a@2	$8.1 \pm 3.1\ 10^{-6}$	0.287 ± 0.036	-52 ± 12
CC-PRY/SPRY	pre-let-7-1a@2	$72 \pm 33\ 10^{-9}$	0.750 ± 0.028	-33.0 ± 2.3
	pre-let-7-1a@2 stem-only	$> 100\ 10^{-6}$	n.d.	n.d.
	pre-let-7-1a@2 loop-only	$4.1 \pm 1.9\ 10^{-6}$	0.809 ± 0.062	-48.9 ± 7.6
	DENV-SL	$15.2 \pm 3.0\ 10^{-9}$ $106 \pm 35\ 10^{-9}$	0.780 ± 0.020 0.080 ± 0.020	-32.4 ± 3.4 -330 ± 100

	Lnczc3h7a	486 ± 77 10^{-9} 8.9 ± 4.5e 10^{-6}	1.25 ± 0.05 0.104 ± 0.063	38.8 ± 5.9 -17 ± 82
CC-PRY/SPRY 381-392 7KA	pre-let-7-1a@2	428 ± 55 10^{-9} 967 ± 11 10^{-6}	0.765 ± 0.028 0.13 ± 0.22	-17.0 ± 1.2 -270 ± 410
CC-PRY/SPRY H505E K508E	pre-let-7-1a@2	484 ± 48 10^{-9} 4.19 ± 0.50 10^{-6}	0.972 ± 0.030 0.196 ± 0.043	-10.2 ± 0.76 -91 ± 18
CC-PRY/SPRY K602E	pre-let-7-1a@2	196 ± 22 10^{-9} 2.54 ± 0.12 10^{-6}	1.08 ± 0.03 0.050 ± 0.043	-3.31 ± 0.53 -270 ± 230
CC-PRY/SPRY K283A K285A	pre-let-7-1a@2	606e ± 124 10^{-9} 16.6 ± 2.1 10^{-6}	1.36 ± 0.06 0.12 ± 0.20	-5.53 ± 0.90 -145 ± 215
CC-PRY/SPRY H505E K508E K602E	pre-let-7-1a@2	790 ± 160 10^{-9} 132 ± 24 10^{-6}	0.973 ± 0.025 0.06 ± 0.29	-2.83 ± 0.49 -300 ± 1400
CC-PRY/SPRY K283A K285A H505E K508E K602E	pre-let-7-1a@2	1.32 ± 0.37 10^{-6} 124 ± 28 10^{-6}	0.972 ± 0.030 0.26 ± 0.12	-0.2 ± 1.7 -210 ± 130
CC-PRY/SPRY Y278A	pre-let-7-1a@2	62.9 ± 6.8 10^{-9} 491 ± 41 10^{-9}	1.04 ± 0.02 0.590 ± 0.017	7.27 ± 0.74 -14.5 ± 1.1
CC-PRY/SPRY Y463S Y476S	pre-let-7-1a@2	252 ± 61 10^{-9} 17 ± 11 10^{-6}	1.42 ± 0.03 0.05 ± 0.10	-8.6 ± 1.2 -290 ± 580

Table2. Filter-binding assays confirm binding to stem-loops

protein	RNA	K_D (M)
CC-PRY/SPRY	pre-let-7-1@2a	10.2 ± 3.8 10^{-9}

	DENV-SL	$1.63 \pm 0.38\ 10^{-9}$
	UNR SL6	$18.1 \pm 2.2\ 10^{-9}$
	UNR SL67	$1.45 \pm 0.47\ 10^{-9}$

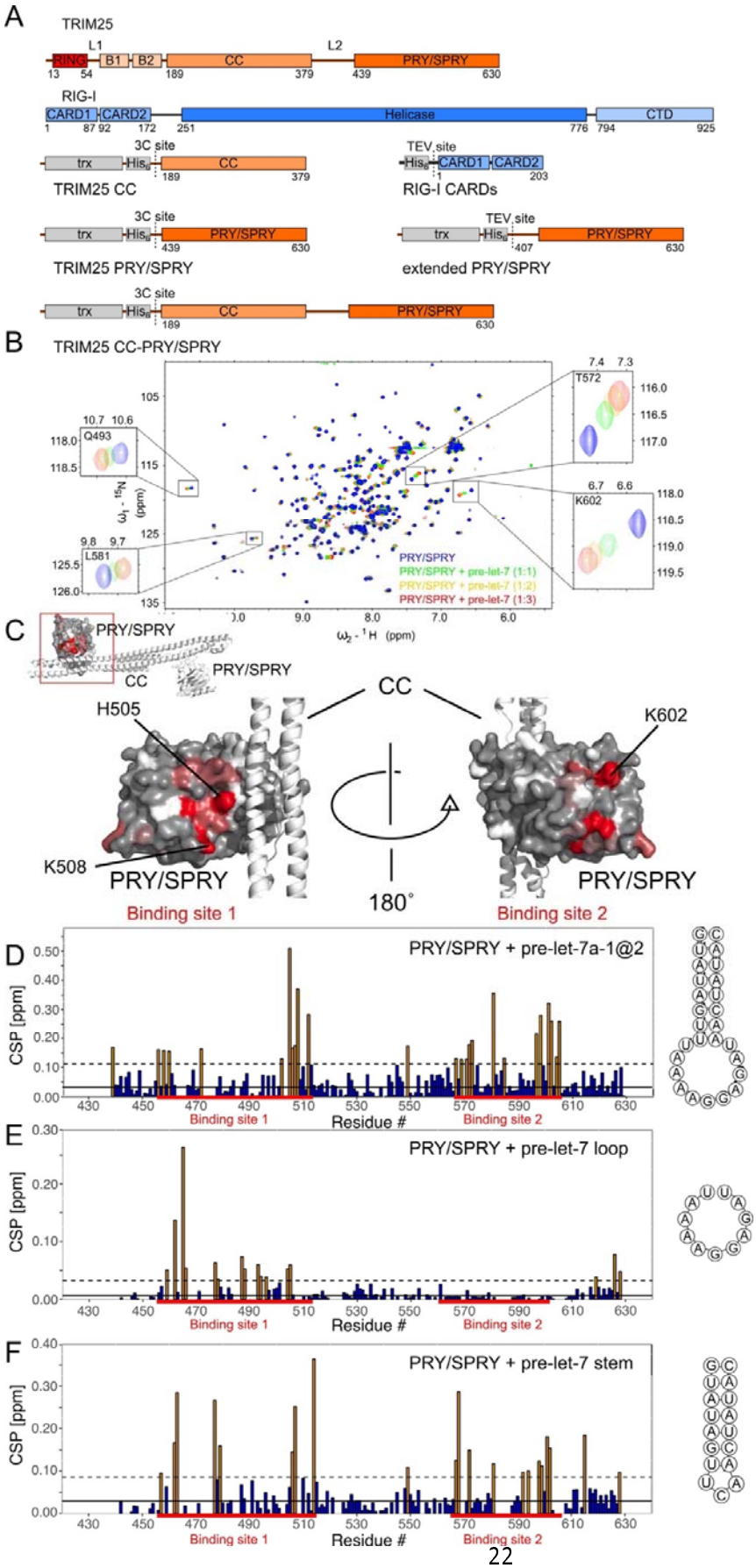

Figure 1. NMR titrations of TRIM25 PRY/SPRY domain and pre-let-7 RNA: **(A)** Domain arrangement of TRIM25 and RIG-I and constructs of both used in this study. Tags were removed by protease treatment prior to the experiments. **(B)** The ^{1}H-^{15}N-HSQC spectra of TRIM25 PRY/SPRY (130 µM) show strong chemical shift perturbations (CSPs) upon addition of pre-let-7 RNA up to a protein:RNA ratio of 1:3. **(C)** Mapping CSPs on the structure (colored as a gradient from gray to red, unassigned residues in white), two strongly affected regions on the structure were identified. The strongest perturbations are located in binding-site-1 close to the interface with the CC, while the second region is found on the opposing face of the domain. Comparison of the CSPs upon binding to full-length pre-let-7 **(D)** with those caused by the loop and stem region shows that the single stranded loop region causes perturbations in a smaller region belonging to binding-site-1 (**E**), while the double-stranded stem affects also the remaining residues on binding-site-1 and binding-site-2 **(F)**. Significantly affected residues are plotted in yellow and the binding sites in the sequence are indicated by red bars. Perturbation close to the C-terminus occur as the C-terminus folds back into the proximity of binding-site-1. CSPs more than one standard deviation (dashed black line) above the average (continuous black line) in C, D, and E are coloured in orange.

A

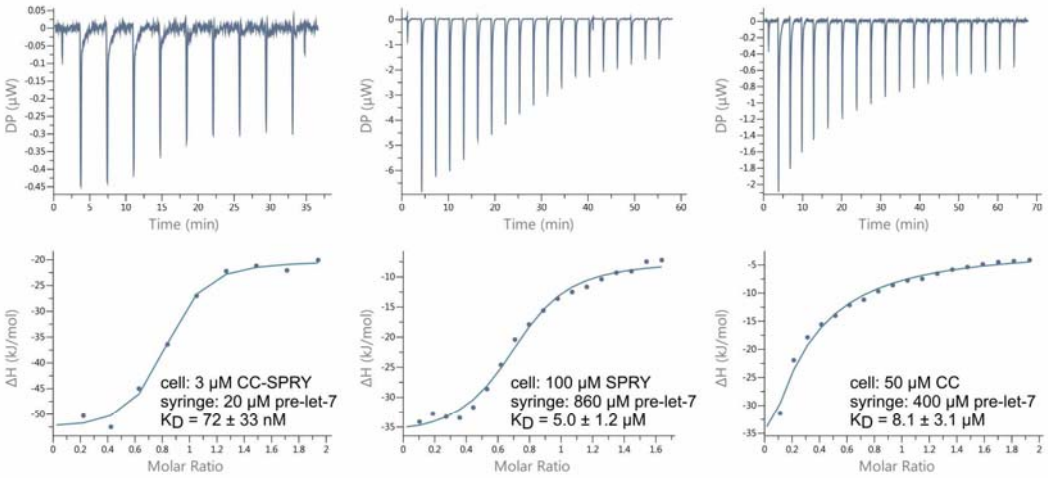

B

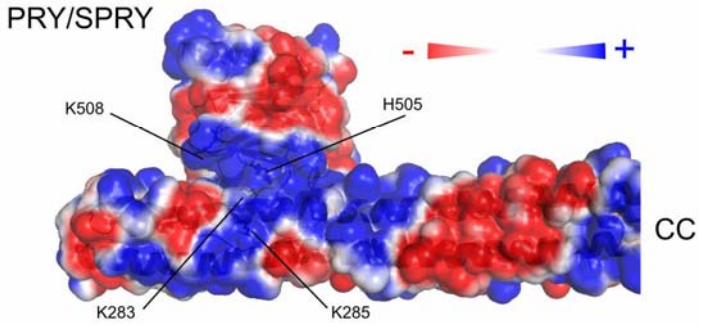

C

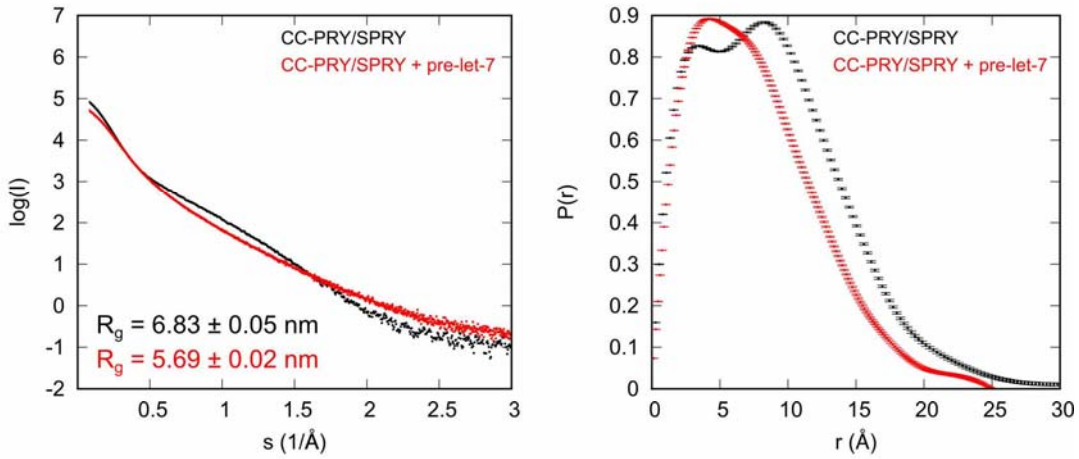

D

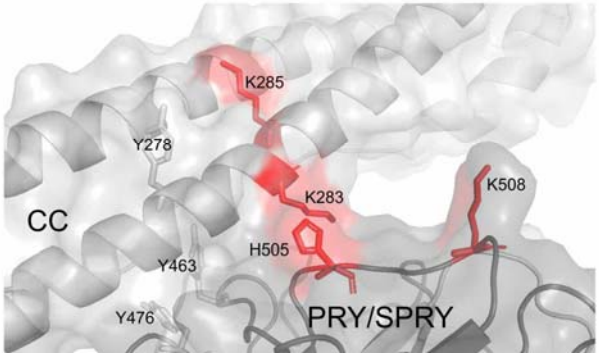

Figure 2. CC and PRY/SPRY domains bind RNA cooperatively: **(A)** Binding isotherms of TRIM25 CC-PRY/SPRY (B) and PRY/SPRY (C) titrated by pre-let-7 show that the PRY/SPRY alone is not sufficient to explain the nanomolar affinity of the longer CC-PRY/SPRY construct. The CC binds pre-let-7 similarly to the PRY/SPRY with micromolar affinity. The thermodynamic parameters of all ITC measurements can be found in Table 1. **(B)** The surface potential of the CC dimer with bound PRY/SPRY (PDB:6FLN) shows that they share a positively charged interface in close proximity to RNA binding-site-1 marked by H505 and K508. **(C)** SAXS curves and pairwise distance distributions for the free TRIM25 CC-PRY/SPRY (black) and its complex with pre-let-7 RNA (red). The distance distribution of the free protein features two maxima, indicating independence of the two domains, whereas the distribution for the RNA-bound complex is much narrower and contains only one peak, indicating a conformational change towards a more compact form. **(D)** K283 and K285 on the positively charged surface of the CC and H505 and H508 on binding-site-1 of the PRY/SPRY form a joined binding interface for RNA. Mutation of the adjacent Y278, a known phosphorylation site of TRIM25 did not affect RNA binding, while mutation of the interface between CC and PRY/SPRY (Y463S Y476S) did, emphasizing the critical role of the CC-PRY/SPRY interaction for RNA-binding.

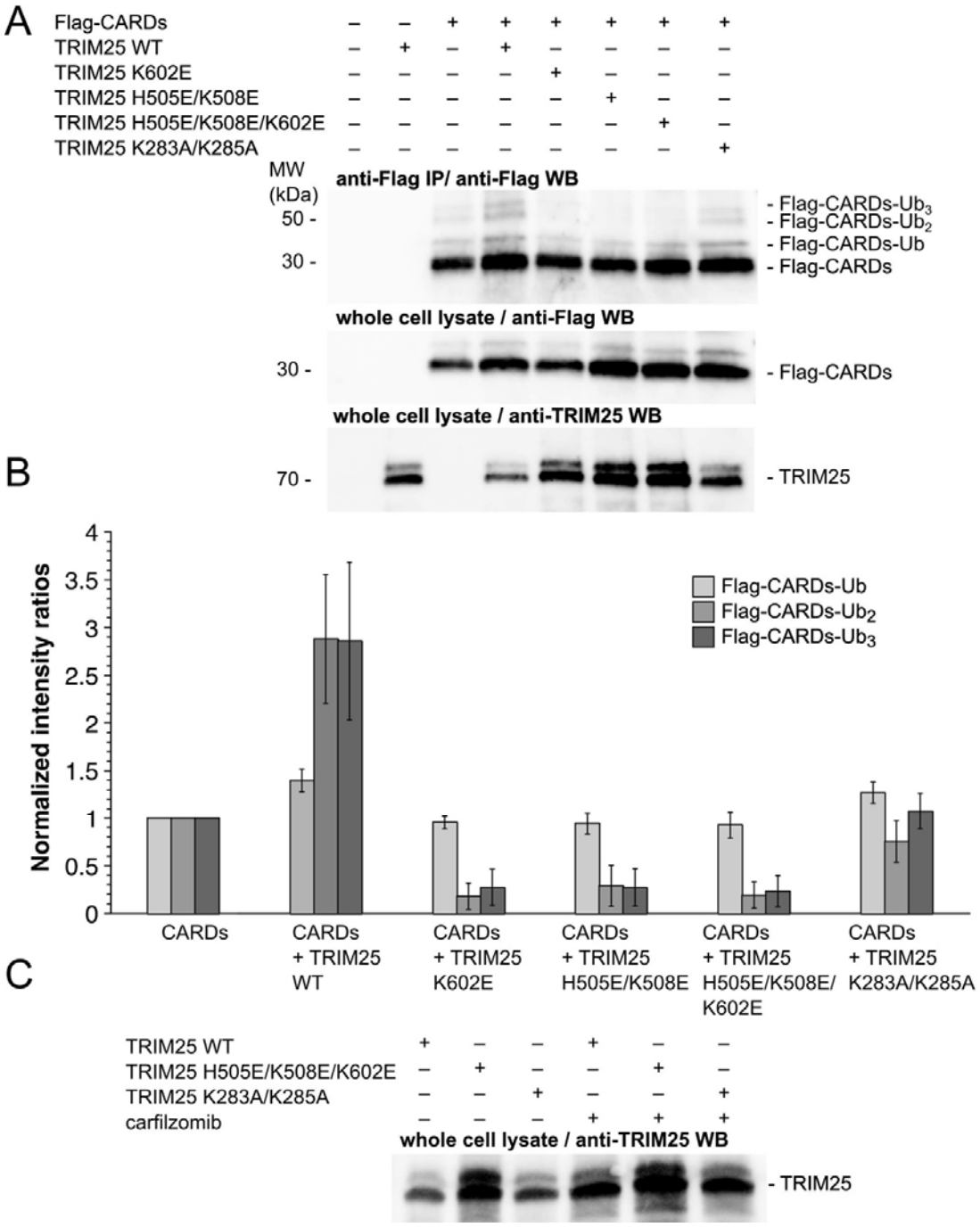

Figure 3. The RNA binding interface is required for RIG-I ubiquitination in cells: **(A)** Flag-tagged RIG-I CARDs were overexpressed with TRIM25 WT or mutants, immunoprecipitated and probed for ubiquitination. **(B)** Quantification of the ratios of ubiquitinated to unmodified CARDs show that only TRIM25 WT increases CARD ubiquitination. The mutants on the PRY/SPRY K602E and H505E/K508E have a dominant negative phenotype and reduce ubiquitination below the level observed without exogenous expression of TRIM25 (N=3-5). **(C)** The mutants on the PRY/SPRY show increased expression levels compared to the wildtype in panel (A). Inhibition of the proteasome

by carfilzomib equalizes expression levels, suggesting that the difference is at least in parts due to reduced auto-ubiquitination.

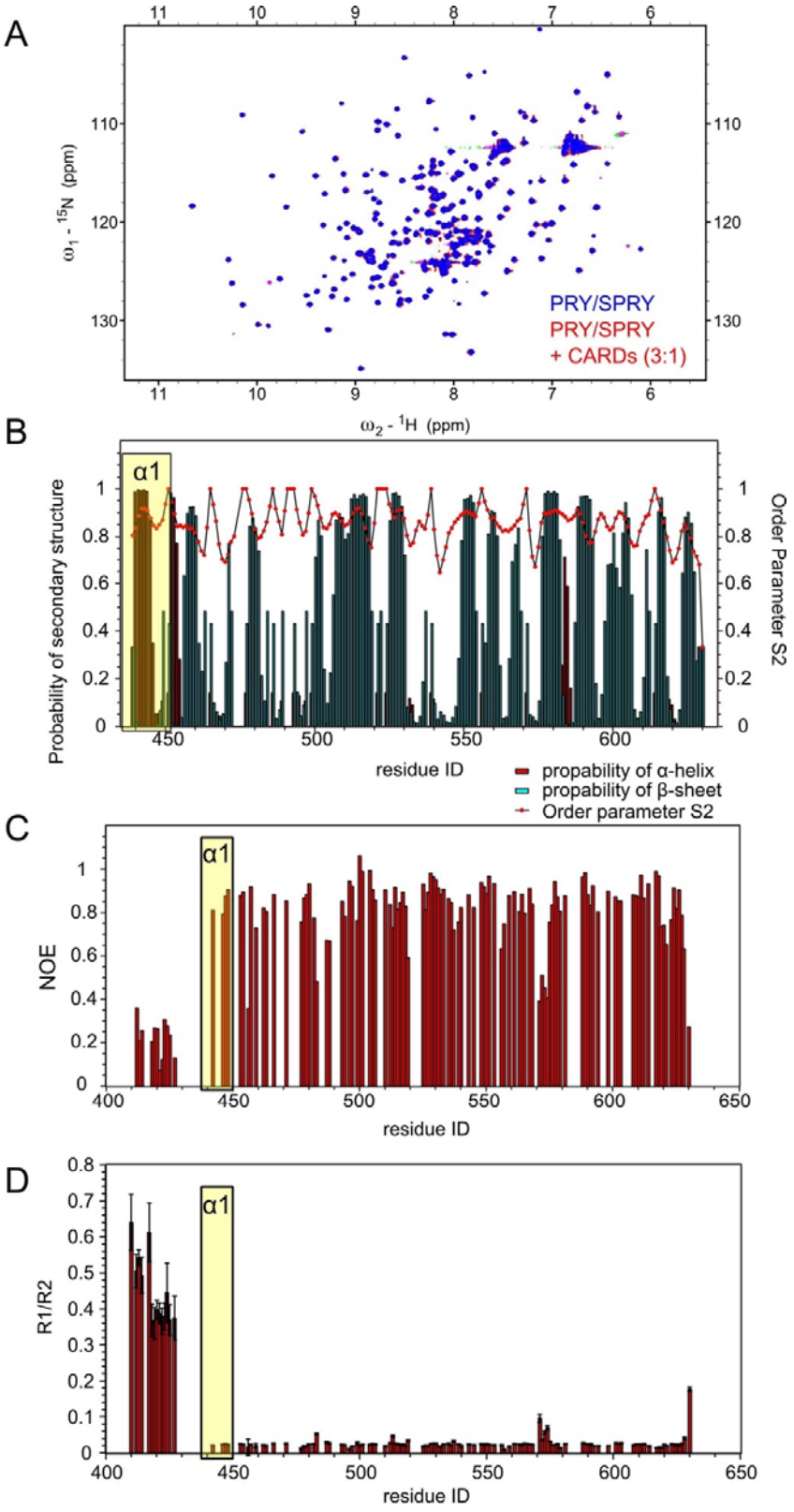

Figure 4. RIG-I interaction and dynamics of helix α1: **(A)** NMR titration of TRIM25 PRY/SPRY by RIG-I CARDs. No CSPs or changes in signal intensity, that would indicate a direct interaction were observed. **(B)** Secondary structure prediction and order parameter for the TRIM25 PRY/SPRY (439-630) based on the previously published assignment (28). In agreement with the crystal structure (PDB:6FLM) the α1 region (marked in yellow) is predicted to form a helix in solution. This is supported by heteronuclear NOEs **(C)**, that show strong correlation of the backbone N-H vectors. This shows that α1 forms a secondary structure. Relaxation measurements **(D)** give information on the backbone dynamics of individual residues. The residues in the α1 region show similar dynamics as the core domain. By contrast the residues belonging to the L2 linker (aa 407-435) are much more dynamic. D'Cruz et al. (42) proposed a mechanism of CARD binding, that would involve rearrangement of helix α1 by a similar helix in the CARD domains. This mechanism is not supported by our data.

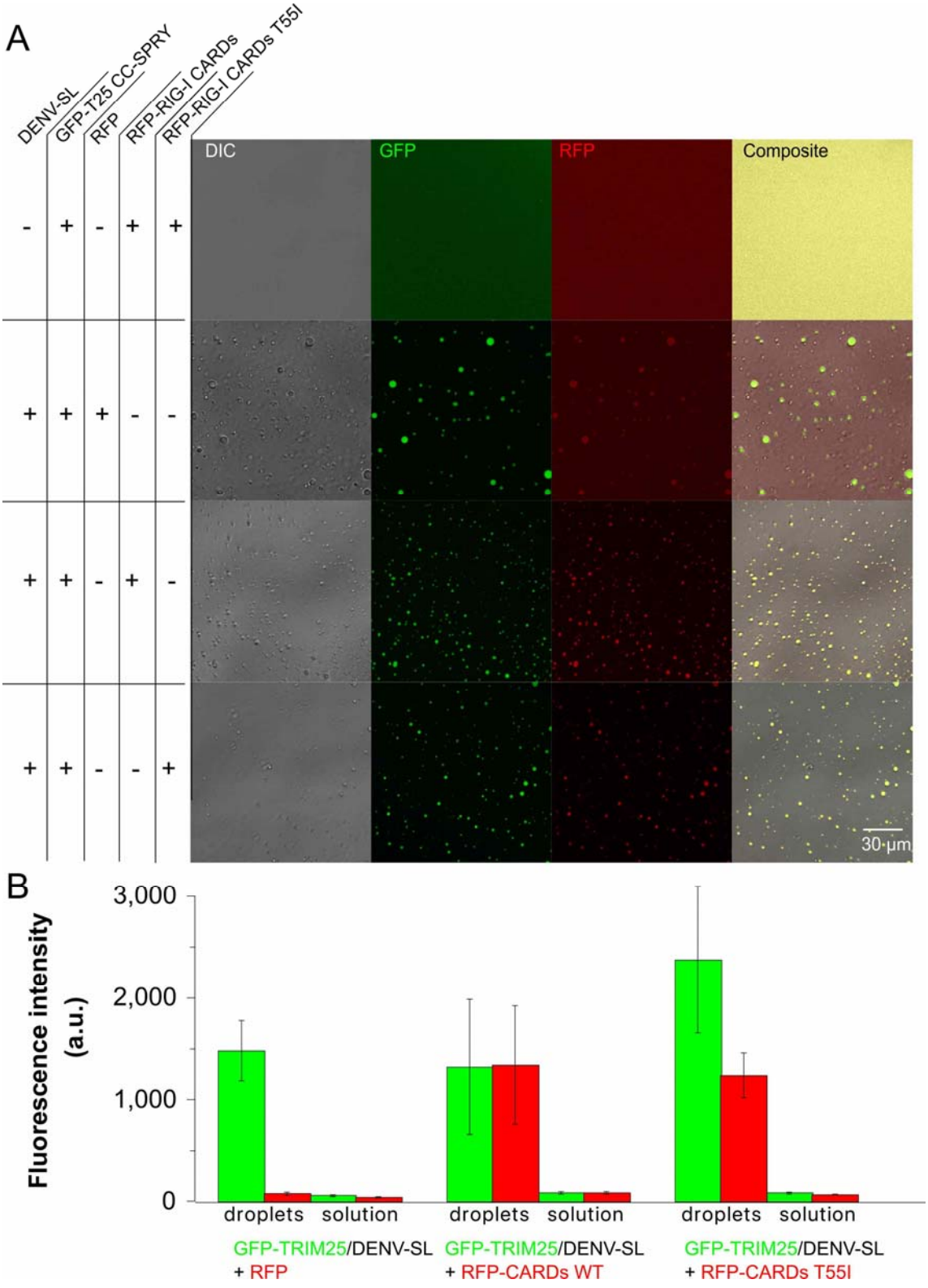

Figure 5. RNA-dependent phase separation of TRIM25: **(A)** Confocal micrographs of GFP-TRIM25 CC-PRY with and without equimolar amounts of DENV-SL. The red channel is used to monitor co-localisation with RFP or RFP-RIG-I CARDs. **(B)** Fluorescence intensities in the droplets were

quantified and show a twenty-fold enrichment of RFP-CARDs in the droplets, while RFP enrichment is less than 2-fold. The T55I mutant reported to reduce the interaction of TRIM25 and RIG-I CARDs (77) has no significant impact on enrichment in the granules.

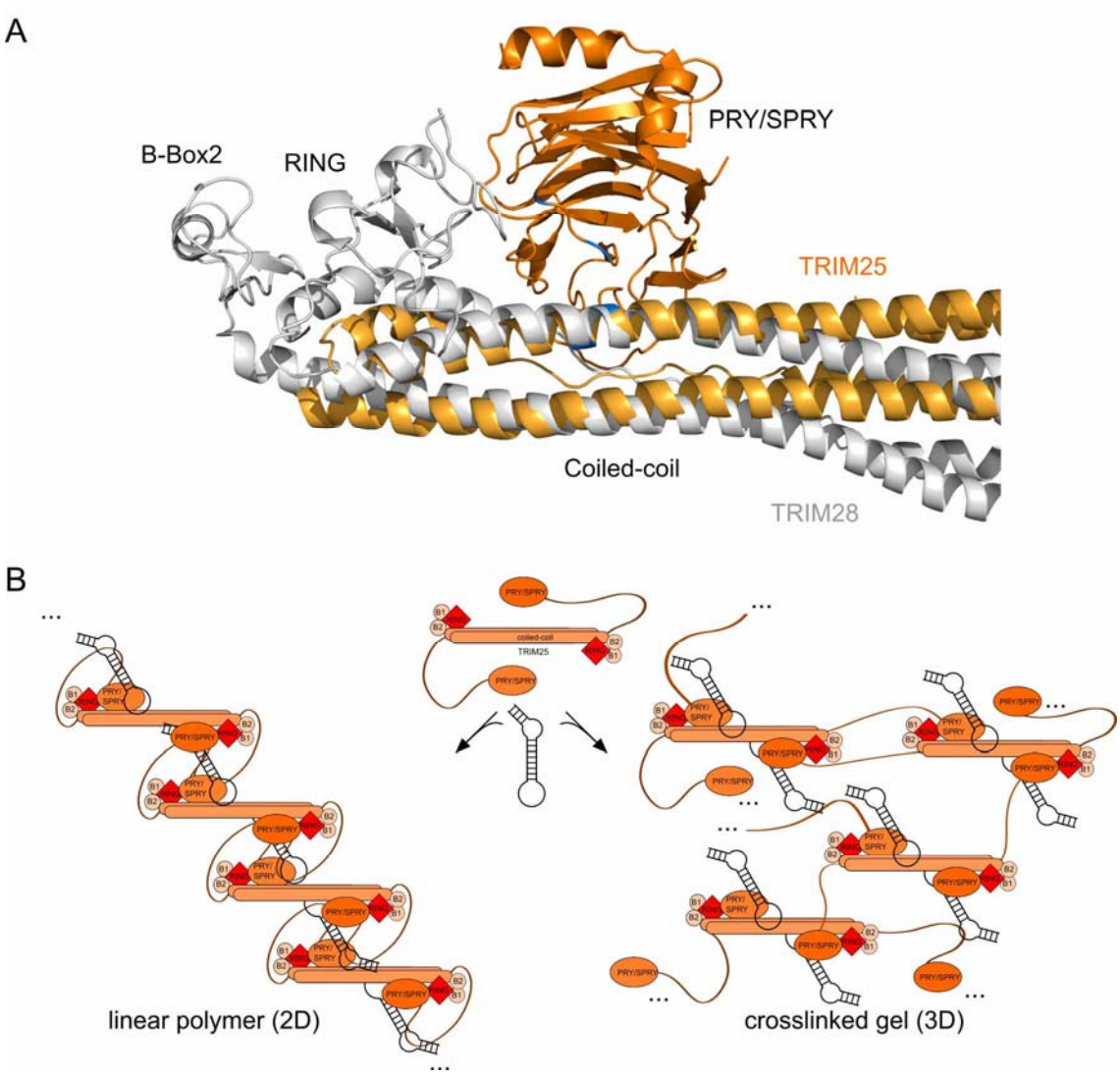

Figure 6. Model of full-length TRIM25: **(A)** Alignment of the crystal structure of the TRIM28 tripartite motif (PDB: 6QAJ) with the TRIM25 CC-PRY/SPRY structure (PDB: 6FLN) (28,56). The alignment suggests that in the context of the full-length protein the RING domain comes in close proximity to the PRY/SPRY domain, explaining the importance of the interaction of CC and PRY/SPRY domain for TRIM25's catalytic activity. Note the close proximity of the RING and the RNA binding site shown in blue. Catalytic activity of TRIM25, but not TRIM28, requires RING dimerization that in this model could only occur by association of two dimers. This could be facilitated by high-concentrations and the

formation of oligomers in phase-separated granules **(B).** Two models could possibly explain phase-separation of TRIM25. A sufficiently long RNA may bind more than one TRIM25 dimer at a time leading to the formation of a linear polymer. Alternatively, intermolecular interactions could be facilitated by binding of the PRY/SPRY of one dimer to the CC of a second dimer, an interaction that is stabilized by RNA. As each dimer could make connections with up to four other dimers a cross-linked gel could form.

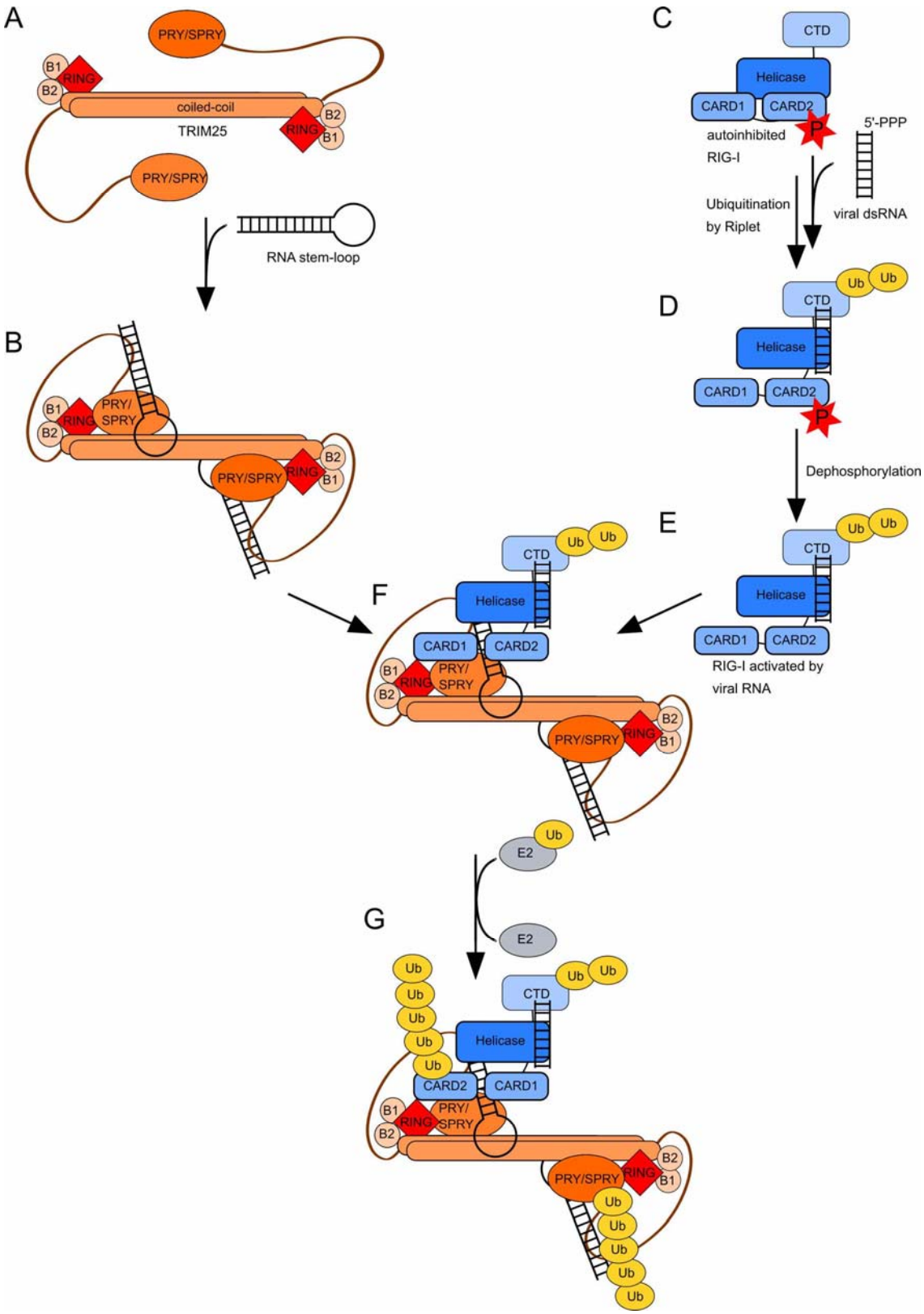

Figure 7. Potential model of RIG-I ubiquitination: **(A)** The CC and PRY/SPRY of TRIM25 in the absence of RNA interact only transiently. **(B)** Upon binding of stem-loop RNA with the PRY/SPRY

domain binding the stem and the base of the loop and the CC likely binding the single-stranded region this interaction is stabilized. The Lysine-rich linker also likely interacts with the stem (26). **(C**) Meanwhile RIG-I remains in the auto-inhibited resting state with the CARDs bound by the helicase domain and requires binding of double stranded viral RNA (20,21), and possibly activation by Riplet ubiquitination (68) **(D)** and dephosphorylation for full activation (78) **(E)**. **(F)** RIG-I is then recruited to TRIM25 by binding the same stem-loop RNA independently of the RIG-I activating double-stranded viral RNA (27). The exact order of events here is speculative. **(G)** TRIM25 poly-ubiquitinates K172 in the second CARD domain of RIG-I. In the absence of a suitable substrate, TRIM25 auto-ubiquitinates, possibly allowing for down-regulation of TRIM25 when not needed. This model assumes that distinct RNAs are necessary for association of TRIM25 and RIG-I and activation of RIG-I, as described for lnczc3h7a (27), but a single RNA might be sufficient for both.